

MICROCOPY RESOLUTION TEST CHART
NATIONAL BUREAU OF STANDARDS-1963-A

AD A123233

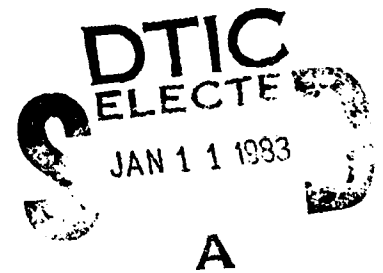
RADC-TR-82-288
Interim Report
November 1982



PHASE CONJUGATE OPTICS

Hughes Research Laboratories

G. J. Dunning
M. B. Klein
R. C. Lind



APPROVED FOR PUBLIC RELEASE; DISTRIBUTION UNLIMITED

DTIC FILE COPY

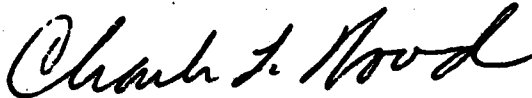
ROME AIR DEVELOPMENT CENTER
Air Force Systems Command
Griffiss Air Force Base, NY 13441

83 01 11 007

This report has been reviewed by the RADC Public Affairs Office (PA) and is releasable to the National Technical Information Service (NTIS). At NTIS it will be releasable to the general public, including foreign nations.

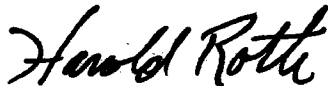
RADC-TR-82-288 has been reviewed and is approved for publication.

APPROVED:



CHARLES L. WOODS
Project Engineer

APPROVED:



HAROLD ROTH, Director
Solid State Sciences Division

FOR THE COMMANDER:



JOHN P. HUSS
Acting Chief, Plans Office

If your address has changed or if you wish to be removed from the RADC mailing list, or if the addressee is no longer employed by your organization, please notify RADC. (ESO) Hanscom AFB MA 01731. This will assist us in maintaining a current mailing list.

Do not return copies of this report unless contractual obligations or notices on a specific document requires that it be returned.

UNCLASSIFIED

SECURITY CLASSIFICATION OF THIS PAGE (When Data Entered)

REPORT DOCUMENTATION PAGE		READ INSTRUCTIONS BEFORE COMPLETING FORM
1. REPORT NUMBER RAD-TR-82-288	2. GOVT ACCESSION NO. AD-A123233	3. RECIPIENT'S CATALOG NUMBER
4. TITLE (and Subtitle) PHASE CONJUGATE OPTICS	5. TYPE OF REPORT & PERIOD COVERED Interim Report 16 Sep 80 - 16 Sep 81	
	6. PERFORMING ORG. REPORT NUMBER N/A	
7. AUTHOR(s) G. J. Dunning M. B. Klein R. C. Lind	8. CONTRACT OR GRANT NUMBER(s) F19628-80-C-0185	
9. PERFORMING ORGANIZATION NAME AND ADDRESS Hughes Research Laboratories 3011 Malibu Canyon Road Malibu CA 90265	10. PROGRAM ELEMENT, PROJECT, TASK AREA & WORK UNIT NUMBERS 61102F 2306J236	
11. CONTROLLING OFFICE NAME AND ADDRESS Rome Air Development Center (ESO) Hanscom AFB MA 01731	12. REPORT DATE November 1982	
	13. NUMBER OF PAGES 108	
14. MONITORING AGENCY NAME & ADDRESS (if different from Controlling Office) Same	15. SECURITY CLASS. (of this report) UNCLASSIFIED	
	15a. DECLASSIFICATION/DOWNGRADING SCHEDULE N/A	
16. DISTRIBUTION STATEMENT (of this Report) Approved for public release; distribution unlimited.		
17. DISTRIBUTION STATEMENT (of the abstract entered in Block 20, if different from Report) Same		
18. SUPPLEMENTARY NOTES RAD-TR Project Engineer: Dr. Charles L. Woods (ESO)		
19. KEY WORDS (Continue on reverse side if necessary and identify by block number) Phase conjugation, image transmission, spatial signal processing, photo refractive materials		
20. ABSTRACT (Continue on reverse side if necessary and identify by block number) The purpose of this program is to study both theoretically and experimentally the use of phase conjugate optics for information processing and image transmission applications. The objectives are to analyze and develop phase conjugation techniques for optical signal processing, to determine the usefulness of phase conjugation for restoring spatial information transmitted over multimode optical fibers, and to study real-time optical convolution and correlation of		

UNCLASSIFIED

SECURITY CLASSIFICATION OF THIS PAGE(When Data Entered)

→ spatially modulated input waves. ✓ The contract was modified after its inception to include a task covering the theoretical and experimental study of materials for use in performing phase conjugation of spatially modulated optical waves.

In the first year of this program we have concentrated our efforts on the study of photorefractive materials for phase conjugation on the restoration of images transmitted through multimode fibers. We have developed a detailed model of the photorefractive effect which will be used as a basis for comparing photorefractive materials for nonlinear phase conjugation. Preliminary results of four materials surveyed indicate that KNbO_3 and BaTiO_3 are the most promising for the applications. Our own experience with BaTiO_3 supports the projected high performance of this material.

In our fiber measurements, we have successfully demonstrated the use of phase conjugation for the restoration of images transmitted through a 1.75-m multimode fiber. The nonlinear material was BaTiO_3 , with a demonstrated nonlinear reflectivity of $\sim 140\%$. This large phase conjugate return was useful in providing large signal levels at the image plane of our system. The preliminary results indicate that a resolution of 5 lines/mm was obtained (compared with a resolution without the fiber of ~ 20 lines/mm). Considerable improvement is expected with more optimized imaging in and out of the fiber.

UNCLASSIFIED

SECURITY CLASSIFICATION OF THIS PAGE(When Data Entered)

TABLE OF CONTENTS

SECTION		PAGE
1	INTRODUCTION	7
2	TECHNICAL PROGRESS	9
	A. Analysis of Mechanisms and Materials for Phase Conjugation	9
	B. Transmission of Images Through Fiber Using Phase Conjugation	18
3	CONCLUSIONS	31
	REFERENCES	33
 APPENDICES		
A	PRELIMINARY REPORT ON THE MATHEMATICS OF PHOTOREFRACTIVITY	A-1
B	LIST OF SYMBOLS, EQUATIONS, TYPICAL VALUES OF PARAMETERS, UNITS, AND CONVERSION FACTORS	B-1
C	BIBLIOGRAPHY - PHOTOREFRACTIVE EFFECT	C-1

DTIC
 COPY
 INSPECTED
 2

Accession For	
<input checked="" type="checkbox"/>	
<input type="checkbox"/>	
<input type="checkbox"/>	
Availability Codes Available and/or Special	
A	

~~3~~
 4

LIST OF ILLUSTRATIONS

FIGURE		PAGE
1	Typical geometry for hologram writing or DFWM in a nonlinear medium. In holographic language, E_1 is the reference writing beam, E_2 is the image writing Beam, E_3 is the readout beam, to E_4 is the signal beam. In the language of DFWM, E_1 and E_3 are the pump beams, E_2 is the probe beam, and E_4 is the signal beam. The parameter Λ is the grating spacing	13
2	Geometer for hologram writing or DFWM in $BaTiO_3$. The beams have the same identification as in Figure 1. The parameter k_g is the grating wave vector	17
3	Demonstration of image transmission through a fiber. (a) Image of Air Force resolution chart at input end of fiber. (b) Output after a single pass through the fiber. (c) Reconstruction of resolution chart after output has been phase conjugated and retraverses fiber	19
4	Schematic of experiment used for image transmission through fibers	21
5	Photograph of experimental apparatus used for image transmission through fibers	22
6	Reconstructed image after double passing the fiber. These preliminary experiments show the resolution is in excess of 5 lines/mm	24
7	Schematic of degenerate four-wave mixing experiments using silica fiber as nonlinear medium	26
8	(a) Phase conjugate oscillator configuration. (b) Output at image plane 3 from phase conjugate oscillator with Air Force Resolution chart in cavity	29

SECTION 1

INTRODUCTION

The purpose of this program is to study both theoretically and experimentally the use of phase conjugate optics for information processing and image transmission applications. The objectives are to analyze and develop phase conjugation techniques for optical signal processing, to determine the usefulness of phase conjugation for restoring spatial information transmitted over multimode optical fibers, and to study real-time optical convolution and correlation of two spatially modulated input waves. The contract was modified after its inception to include a task covering the theoretical and experimental study of materials for use in performing phase conjugation of spatially modulated optical waves.

The transmission of a "picture" through a multimode fiber suffers from several problems, two of which are modal dispersion and mode mixing. It is well known that the process of phase conjugation - that is, passing a spatially modulated wave through a fiber, conjugating, and then retransmitting the beam back through the same fiber - can compensate for these effects and produce a restored image.

Further, the ability of one nonlinear technique, degenerate four-wave mixing (DFWM), to perform the multiplication of two (or three) input signals in a nonlinear medium provides the capability of generating the optical convolution or correlation of spatially modulated waves.

The use of a nonlinear optical process to generate the optical correlation/convolution is essentially a generalized Vander Lugt Holographic filter technique in which a nonlinear medium operating as a four-wave mixer replaces a conventional holographic film recording. The key advantage of such a system is that the "hologram" may be written and played back almost instantaneously (i.e., real-time signal processing can be performed).

In the first year of this 30-month program we have concentrated our efforts on the study of photorefractive materials for phase conjugation and on the restoration of images transmitted through multimode fibers. We have developed a detailed model of the photorefractive effect which will be used as a basis for comparing photorefractive materials for nonlinear phase conjugation. Preliminary results of four materials surveyed indicate that KNbO_3 and BaTiO_3 are the most promising for the desired applications. Our own experience with BaTiO_3 supports the projected high performance of this material.

In our fiber measurements, we have successfully demonstrated the use of phase conjugation for the restoration of images transmitted through a 1.75-m multimode fiber. The nonlinear material was BaTiO₃, with a demonstrated nonlinear reflectivity of ~140%. This large phase conjugate return was useful in providing large signal levels at the image plane of our system. The preliminary results indicate that a resolution of 5 lines/mm was obtained (compared with a resolution without the fiber of ~20 lines/mm). Considerable improvement is expected with more optimized imaging in and out of the fiber.

SECTION 2

TECHNICAL PROGRESS

A. ANALYSIS OF MECHANISMS AND MATERIALS FOR PHASE CONJUGATION

A large number of nonlinear mechanisms have been proposed or demonstrated which have promise for phase conjugation of spatially-modulated optical signals via degenerate four-wave mixing (DFWM). We have performed a preliminary survey of these mechanisms along with the performance of specific materials; the results are given in Table 1. Several of the tabulated materials have the desirable properties of requiring modest (CW) pump power levels and having response times in the millisecond or sub-millisecond region. It is expected that most of the materials should operate at spatial frequencies approaching 1000 lines/mm (1 μ m resolution in the material), and thus be suitable for handling high spatial bandwidth signals.

Among the mechanisms and materials listed in Table 1, we have chosen to devote our initial attention to photorefractive materials. The specific advantages of these materials are that they operate over a relatively wide frequency range at modest CW power levels and have response times which approach the required value of 1 msec. Two photorefractive materials with particular high promise are BaTiO₃ (demonstrated high efficiency), and KNbO₃ (fast response with moderate efficiency), and these have been included in Table 1.

We have undertaken a detailed study of the photorefractive effect, whose goal is the determination of optimum materials and configurations for phase conjugation of spatial modulated waves via DFWM. As a first step, a literature survey was conducted; a list of all references encountered and the materials studied is given in Appendix C. During the course of our literature survey, we collected pertinent performance parameters for a number of prominent materials; these are tabulated in Table 2. The intercomparison of materials should be considered only qualitative, because experimental conditions varied among the cited references, and often were not optimized for the tabulated parameter. In Table 2, the sensitivity S is related to the writing of a holographic grating, and is the change in refractive index per unit of absorbed energy. An alternative parameter for characterizing the sensitivity in a two-beam interference experiment is the writing energy required to obtain 1% diffraction efficiency, or the energy to write a grating with 1/e of the saturation efficiency. In Table 2 we have not made a distinction between those two definitions, although they can lead to differences of as much as an order of

Table 1. Mechanisms and Materials for Phase Conjugation of Spatially Modulated Signals via Degenerate Four Wave Mixing

Nonlinear Mechanism	Typical Material	Wavelength, μm	Typical Operating Power level, w/cm^2	Response Time	Typical DFWM Reflectivity	Comments
Photorefractive effect	BaTiO_3 KNbO_3	0.45-0.65 0.45-0.65	1 1	10-100 msec 1-10 msec	150.0% 30.0%	High quality samples hard to obtain
Saturable absorption	Rhodamine 6G Sodium Ruby Eosin	0.48-0.54 0.59 0.45-0.52 0.48-0.54	10^6 (pulsed) 50 100 1	10 nsec 10 nsec 4 msec 4 msec	1.0% 100.0% 3.0% 0.1%	High power required narrow band
Plasma-induced grating	CdS Si	0.53 1.06	10^6 (pulsed) 10^6	1 sec 1 sec	30.0% 150.0%	High power required High power required
Inertial grating	Liquid solvent with dissolved dye Liquid crystal near phase transition	0.4-1.2 0.4-1.5	0.1	10 msec 100 msec		Prefers pulsed operation Untested
Molecular orientation in liquid crystal near phase transition	NBBA	0.4-1.2	1	1 sec	10.0%	Relatively slow
Optically-induced grating in liquid crystal light valve	NBBA	0.4-1.0	5×10^{-5}	8 sec	6.0%	Slow, imperfect conjugation
Artificial kerr medium	Latex spheres in water	0.4-1.5	5×10^3	140 msec	0.5%	High power required
Light-induced surface grating	Epoxy resin with dissolved dye	0.4-1.5	0.4	10 msec	30.0%	Quality of conjugation unknown

Table 2. Performance Parameters for Prominent Photorefractive Materials.
The Parameter Λ is the Grating Spacing.

Photorefractive Material	Sensitivity $S = \frac{dn}{dW}$ cm^3/J	Writing Energy		Response Time at 1 W/cm^2 sec	DFWM Reflectivity	Transport Mechanisms		
		Zero Field J/cm^2	Field E J/cm^2			Diffusion	Bulk Photovoltaic Effect	Drift
LiNbO_3	$2 \times 10^{-5}(\text{a})$	$0.01(\text{b})$			$10^{-2}(\text{c})$	Important for $\Lambda < 1 \mu\text{m}$	Weak	Moderate
$\text{LiNbO}_3:\text{Fe}$	$3 \times 10^{-4}(\text{d})$	$\begin{cases} 0.3(\text{n}) \\ 0.1(\text{b}) \end{cases}$				Important for $\Lambda < 1 \mu\text{m}$	Strong	Moderate
BaTiO_3		$0.1(\text{e},\text{b})$	$0.001 \text{ to } 10 \text{ kV/cm}(\text{e})$	$\begin{cases} 0.4(\text{g}) \\ 0.5(\text{h}) \end{cases} E = 0$	$20(\text{f})$		Moderate	Strong
KNbO_3	$10^{-4}(\text{a},\text{d})$			$0.5(\text{a})$		Important for $\Lambda < 1 \mu\text{m}$	Weak	Strong
$\text{KNbO}_3:\text{Fe}$	$5 \times 10^{-2}(\text{d})$			$\begin{cases} 0.6(\text{a}) \\ 0.01(\text{j}) \end{cases}$	$10^{-1}(\text{j})$		Strong	Strong
BSO	$10^{-1}(\text{d})$		$0.001 \text{ to } 10 \text{ kV/cm}(\text{k})$	$0.03(\text{k})$	$10^{-3} \text{ to } 6 \text{ kV/cm}(\text{m})$	Important for $\Lambda < 1 \mu\text{m}$	Absent	Strong

- a. Gunter and Micheron (1978)
- b. Staebler and Phillips (1974)
- c. Kukhtarev and Odoulov (1980)
- d. Gunter and Krumin (1980)
- e. Kratzig (1980)
- f. Lam, et. al. (1981)
- g. Townsend and LaMacchia (1970)
- h. Feinberg, et. al. (1980)
- i. Feinberg and Hellwarth (1981)
- j. Gunter Preprint (1981)
- k. Peltier and Micheron (1977)
- m. Huiquard et. al. (1979)

magnitude in the tabulated value. The response time is inversely proportional to the input power (as discussed below), and is the time required to write a grating with $1/e$ of its saturated efficiency. There have been only a few experiments on DFWM in photorefractive materials; the observed signal-to-probe reflectivity is also tabulated in Table 2. Finally, we have listed the relative importance of the three transport mechanisms which participate in forming the phase grating and which determine the relative spatial phase with respect to the interfering optical fields. These mechanisms are all accounted for in the model described below.

Under subcontract to HRL on this program, Dr. Marshal Sparks has developed a detailed model of the photorefractive effect whose purpose is to suggest experiments for the measurement of critical parameters, and to identify preferred materials (and optimum experimental conditions). At this stage the model considers the interference of two beams to write a simple holographic grating (see Figure 1). The presence of a third "readout" beam simultaneous with the "writing" beams (as is present in a typical DFWM experiment), and the dynamic influence of these beams on the grating has not been considered. The model in its present form can provide information on the writing energy, response time and spatial resolution for a given system; further refinement is required to model the nonlinear reflectivity in a typical DFWM experiment. A preliminary manuscript of Dr. Sparks' written contribution is given in Appendices A and B.

The theory which has been developed provides both transient and steady state solutions to the system equations for diffusion, drift and the photo-voltaic effect acting individually or simultaneously. In the model, the photorefractive material is an insulator with N_D optical levels per cubic centimeter in the electronic bandgap. The levels are sufficiently deep that they are not thermally excited into the conduction band. The levels are called optical-donor levels because electrons from these levels are photoexcited into the conduction band. The density of the optical-donor levels that are filled with electrons is N_e and the density that are unfilled is N_+ . For example, N_e could be the Fe^{2+} density in lithium niobate, N_+ the Fe^{3+} . In general, there are many filled levels N_e and many empty levels N_+ . The ratio N_e/N_+ can be varied by oxidizing or reducing the sample or by doping the compensating impurities. In order to make the crystal have charge neutrality when growing, there must be negative impurities or imperfections present to compensate for the positive

11368-6

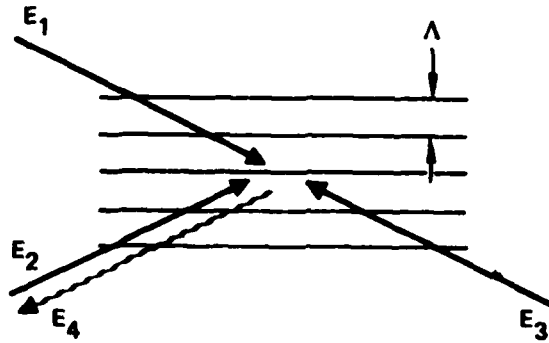


Figure 1. Typical geometry for hologram writing or DFWM in a nonlinear medium. In holographic language, E_1 is the reference writing beam, E_2 is the image writing Beam, E_3 is the readout beam, and E_4 is the signal beam. In the language of DFWM, E_1 and E_3 are the pump beams, E_2 is the probe beam, and E_4 is the signal beam. The parameter Λ is the grating spacing.

charges of the iron. The density of these levels that compensate for the extra positive charge of the Fe^{3+} is equal to the value N_{+0} of N_+ before the irradiance is turned on. Subscript zeros denote the values of parameters at $t = 0$, the time at which the irradiance is turned on.

Holes are neglected for simplicity. Electrons are generated from the filled optical-donor levels to the conduction band by the irradiance and recombine with empty optical-donor levels. Trapping is neglected in this model. We use the common photoconductivity terminology that electrons in traps can be thermally re-excited into the conduction band. Thus, the capture of electrons by the empty optical-donor levels is called recombination, rather than trapping. This recombination into the optical-donor levels is not to be confused with recombination of holes and electrons across the gap.

The emphasis to date has been on lithium niobate because there is more information available on this material than on other materials, some of which may be better candidates for the intended applications. This information is useful in establishing the validity of the theory, which will be done to the extent possible before applying the theory to other materials such as BaTiO_3 and KNbO_3 .

The appropriate system equations were identified and solved in the important limiting cases of short drift distance and long drift distance (with respect to the grating-spacing distance, Λ) and of short times and steady-state.

the conditions for short- and long-diffusion distances are different for the short-time- and steady-state- limits.

Simple physical explanations of the results were developed. The grating phase shifts for the various combinations of drift and diffusion and of short- and long-transport distances were explained without mathematical analysis.

Discrepancies between the key results of Amodei¹ and of Kukhtarev and coworkers² and simple results obtained from general principles were discovered and resolved. Amodei's assumption that saturation and depletion are negligible is inconsistent with the steady-state solution, which is not obtained in the limit of negligible saturation and depletion. Kukhtarev's solution for the grating field E_g is not valid for the case of negligible diffusion and open circuit (for which $E_g = 0$), but is valid in the presence of a small amount of diffusion.

There are several characteristic times in the photorefractive effect that come out of the theory, the most important of which is the dielectric relaxation time τ_{di} , which controls the writing and erasing of the holographic grating in all cases (diffusion-, applied field-, and bulk photovoltaic effect-controlled). The dielectric relaxation time is given by (see Appendix A, Equation (3.7)):

$$\tau_{di} = \frac{\epsilon}{4\pi\sigma} = \frac{\epsilon}{4\pi e\mu\langle n \rangle} \quad (1)$$

where ϵ is the relative dielectric constant, μ is the electron mobility and $\langle n \rangle$ is the spatial average of the conduction band electron density. A rate equation solution for $\langle n \rangle$ gives

$$\langle n \rangle = \frac{\sigma_D \langle I \rangle N_{eo}}{\gamma_r \hbar \omega} \quad (2)$$

where σ_D is the optical cross section, $\langle I \rangle$ is the spatially-average intensity, and γ_r is the recombination rate. We note that γ_r is given by

$$\gamma_r = v_{th} S N_{+0} \quad (3)$$

where v_{th} is thermal velocity of the conduction band electrons, and S is the capture cross section. Substituting Equations (2) and (3) into Equation (1) gives

$$\tau_{di} = \frac{\epsilon \hbar \omega v_{th} S N_{+0}}{4\pi e \mu \sigma_D \langle I \rangle N_{eo}} \quad (4)$$

Several important conclusions can be drawn from Equation (4). We first note that for a given experiment, the response time is inversely proportional to the average intensity, and the product $\tau_{d1}\langle I \rangle$ is a constant (equal to the writing energy of the grating). One important means for diminishing the response time is to chemically treat the crystal ("reduction") to increase the ratio (N_{e0}/N_{t0}) of filled to unfilled levels. The ratio N_{e0}/N_{t0} , not the individual values of the densities, determines the writing and erasing speed (for fairly wide ranges of N_{e0} and N_{t0}). In comparing candidate photorefractive materials, Equation (4) points out the importance of selecting materials with small values of the quantity $S/\mu\sigma_D$. One difficulty to overcome is the lack of information on the levels involved, as well as their optical capture cross sections.

In the experimental phase of our materials study, we have carefully characterized BaTiO_3 to determine the suitability of this material for use on this program. To this end we have performed two-wave mixing and four-wave mixing experiments. The two-wave experiments have led to the determination of the sense of the c-axis direction, and have shown a 50% energy transfer from one beam to another. In these experiments, the angle θ between the grating k vector (\bar{k}_g) and the positive c-axis direction (see Figure 2) was varied between 0° and 20° , with the highest energy transfer obtained at the largest angle. On the basis of this performance, we are still determining if two-wave mixing has applicability for image amplification on this program.

The DFWM configuration has been used for most of our image transmission experiments in fibers and it is expected to be used for the convolution/correlation experiments. To this end we have measured the DFWM reflectivity as a function of several parameters including angle between pump/probe, polarization of the beams, direction of c-axis, intensity of the beams, beam diameter, etc. Because of the slow time response of the material (~ 0.1 sec at the power levels of our experiment) it was necessary to perform these experiments on a vibrationally isolated table.

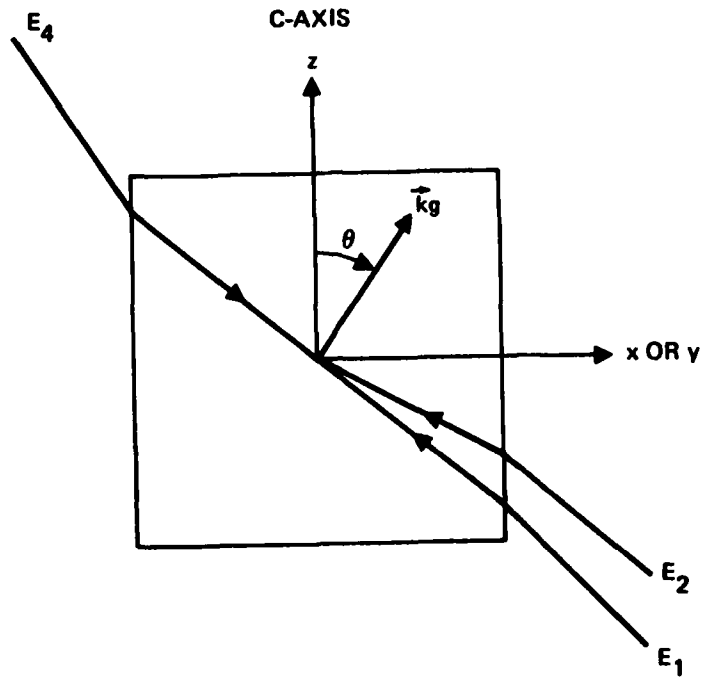


Figure 2. Geometry for hologram writing or DFWM in BaTiO_3 . The beams have the same identification as in Figure 1. The parameter k_g is the grating wave vector.

The important results of the experiments are that the highest nonlinear reflectivity is obtained with the grating k vector inclined to the positive c -axis direction, as predicted by Feinberg et. al.³ In our experiments we were only able to obtain a 20° angle, due to the cut of the BaTiO_3 crystal, and its large refractive index. Published calculations give an optimum angle of $\sim 50^\circ$, although the reflectivity at 20° is reduced by only a factor of three. The largest reflectivity which we have measured is 133%, which allows direct visual observation of the reconstructed images at modest laser power levels.

B. TRANSMISSION OF IMAGES THROUGH FIBERS USING PHASE CONJUGATION

During this portion of the program we have been investigating the transmission of images through multimode fiber waveguides using optical phase conjugation or wavefront reversal techniques. The transmission of spatial information through fibers is degraded due to mode mixing and modal dispersion. By making use of the wavefront reversal property of nonlinear optical techniques we can compensate for these effects. In our preliminary experiments an image was transmitted through a fiber, conjugated, and made to retrace the same fiber, resulting in the reconstruction of the image at the input end of the fiber. For this to be a useful forward transmission technique, operation with two nearly identical fibers will be required. The image will be transmitted through the first fiber, conjugated and then transmitted through the second fiber which reconstructs the image at its output.

The preliminary demonstration was accomplished by utilizing a multimode (85 μm diameter, 1.75 m long) step-index fiber. The output of an argon laser (5145 \AA) was transmitted through a portion of an Air Force resolution chart and imaged at the input end of the fiber. The fiber output was directed into a crystal of barium titanate (BaTiO_3) in which DFWM was used to generate the phase conjugate signal. The phase conjugate signal then retraversed the same fiber and reconstructed the image of the resolution chart. The results of this experiment are shown in Figure 3. The first photograph shows the input image of an Air Force resolution chart. The second photograph shows the output at the end of the fiber. The output is typical of a highly multimode fiber where a large number of modes are excited. From the output, it is impossible to discern that any spatial information has been transmitted through the fiber. The reconstructed image after double passing the fiber is shown in the last photograph.

11210-2R2

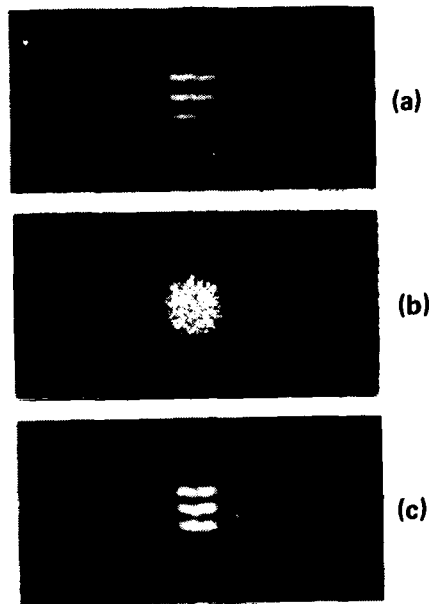


Figure 3. Demonstration of image transmission through a fiber. (a) Image of Air Force resolution chart at input end of fiber. (b) Output after a single pass through the fiber. (c) Reconstruction of resolution chart after output has been phase conjugated and retraverses fiber.

The geometry employed for the four-wave mixing experiments in this work is shown in Figure 4. It consists of two counterpropagating pumps (E_f, E_b) and a probe wave (E_p) (which is the beam with the image information imposed on it) incident on the nonlinear medium. These beams interact to generate the phase conjugate signal (E_s). A photograph of the actual apparatus is shown in Figure 5.

The argon-ion laser (5145 Å) used as the illumination source has an intracavity prism and etalon for single longitudinal mode operating giving coherence lengths on the order of 10 m. In order to have useful interference between the pump and probe the coherence length of the laser must be comparable to the path length differences encountered in the experiment. For our experiments the probe path length is longer than the path length of the pump beams by at least the length of the fiber, thus requiring a ~ 10 m coherence length.

The laser output is continually monitored by a scanning Fabry-Perot etalon. Because of crystal orientation, p-polarization of the input beams is required in our experiments. Therefore, a $\lambda/2$ plate and Faraday rotator were used to rotate the plane of polarization of the argon laser. The Faraday rotator was also used in conjunction with a polarizer to prevent any return beams from entering the laser and destroying single mode operation. The beam splitter, BS2, picks off the pump beams. A 100 cm f.l. lens was used to reduce the pump beam size in the crystal. The beam splitter, BS3, picked off a secondary probe signal which was used to optimize the crystal orientation. The beam splitter, BS4, was used to generate the individual counterpropagating pumps. The pumps typically have a power ratio of 2:1. The throughput of the beam splitter, BS2, is used to obtain the probe used in the fiber. This probe beam was expanded by a beam expanding telescope to illuminate the Air Force resolution chart. Following the resolution chart is a beam splitter BS6. This element is used to pick off the return signal which forms an image on a sheet of cardboard. The image plane is the exact same distance from the beam splitter as the original Air Force chart. An f.l., 7.6 cm focal length relay lens was used to capture the light diffracted by the patterns of the resolution chart. This diffracted light would otherwise miss the entrance aperture at the microscopic objective. The microscope objectives are 7X, 0.20

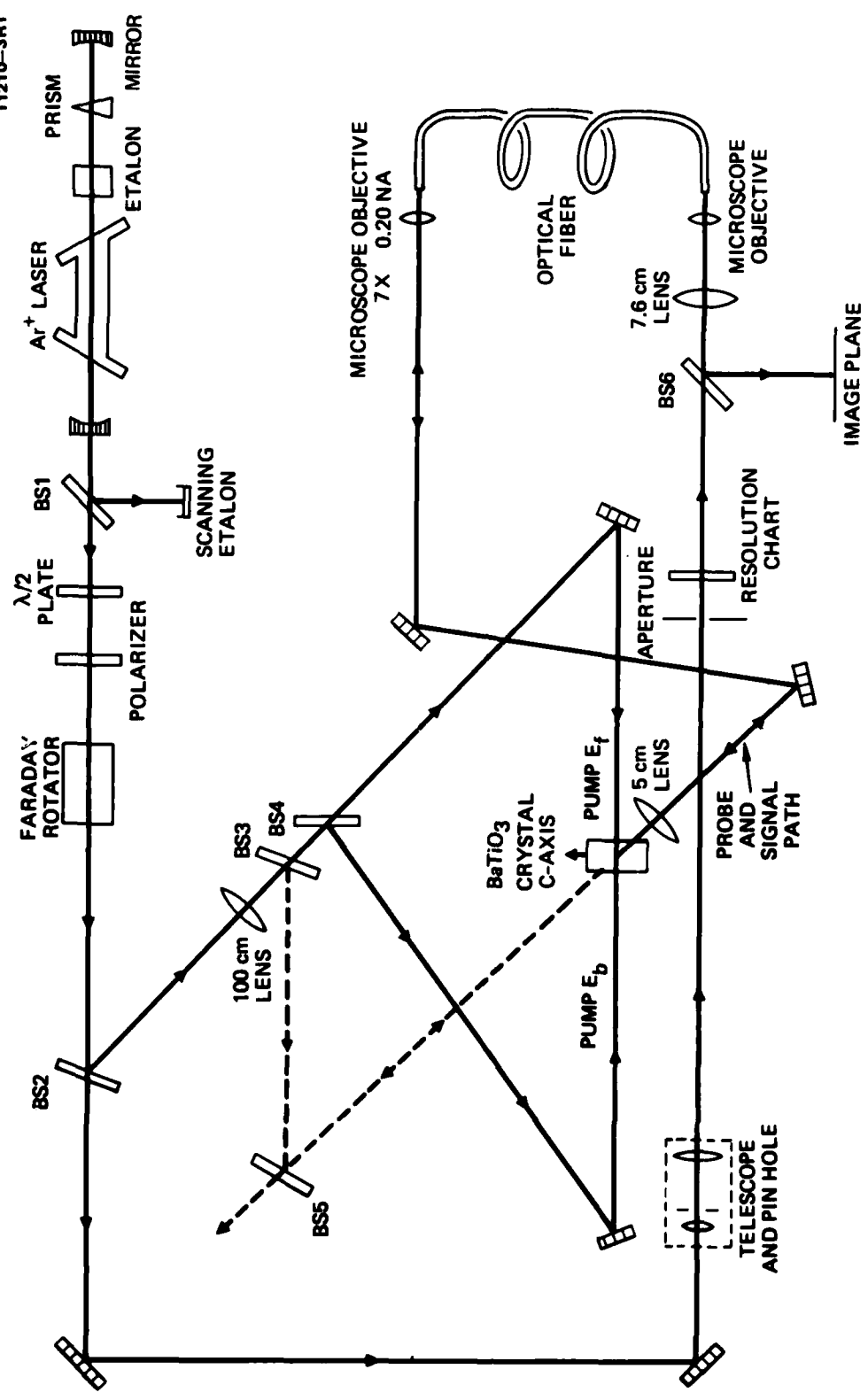


Figure 4. Schematic of experiment used for image transmission through fibers.

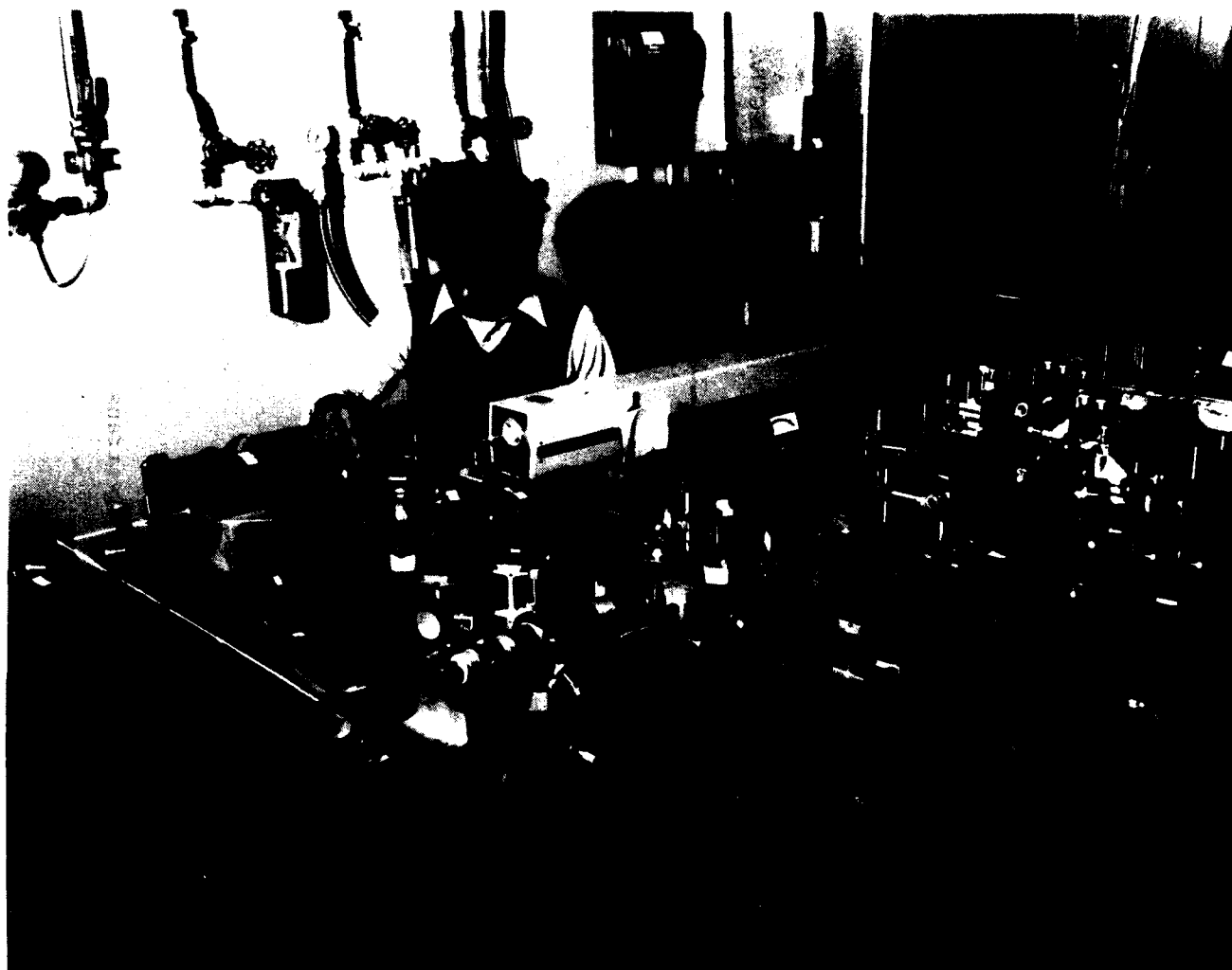


Figure 5. Photograph of experimental apparatus used for image transmission through fibers.

N.A. The first microscope objective couples the light into the fiber. The fibers are held by a unique Hughes designed fiber holder and fiber assembly which has five degrees of freedom: x - y - z translation and azimuthal and polar rotations.

In our studies we have used four types of fibers which are representative of the various fiber designs. The first fiber is a "single" or lower mode number fiber from Bell Laboratories. It has a step index with a core diameter of 8.5 μm and a numerical aperture, N.A., of 0.052. There are several lengths, the longest being 60 m. At the wavelengths of interest, $\sim 5000 \text{ \AA}$, we can propagate three discrete modes, of which two are degenerate. The number of modes M is given by $M = k^2 a^2 (\text{N.A.})^2$, where a is the core diameter. The second fiber is a multimode graded index fiber supplied by ITT. The core diameter is 50 μm , the N.A. is 0.25 and the length is 6 m. Theoretically, approximately 10^4 modes can propagate in this fiber at the wavelengths of interest. The third fiber is a Corning 85 μm step index fiber (N.A. = 0.184) which is 1.75 m in length. It also can propagate $\sim 10^4$ modes. The fourth fiber is a multimode step index fiber supplied by Quartz Products. The core diameter is 200 μm and the N.A. is 0.20. This fiber can support on the order of 10^5 modes. We have measured the properties of fiber transmission at three different wavelengths, 4131 \AA , 5145 \AA , and 6471 \AA so that we can optimize both the wavelength and fiber for a particular experiment. As mentioned for the initial image transmission studies we used the Corning 85 μm fiber.

A second microscope objective (see Figure 4) quasicollimates the output beam from the fiber. A 5 cm focal length lens is then used to reduce the probe beam to a diameter smaller than the diameter of the pump beams inside the crystal. The pumps typically make an angle of 75° with respect to the c-axis and the probe, an angle of 68° . This implies that the angle of the grating normal is 18° with respect to the c-axis. The highest reflectivity is obtained when the grating vector is inclined to the positive c-axis direction, as predicted by Feinberg et. al.³ Using this geometry we have obtained reflectivities in excess of 133%.

These large returns have enabled us to easily reconstruct the image and show image amplification. At present we have been able to resolve better than 5 lines/mm (100 μm spacing), see Figure 6. (The resolution of the optical system



Figure 6. Reconstructed image after double passing the fiber. These preliminary experiments show the resolution is in excess of 5 lines/mm.

without the fiber is 20 lines/mm; and we have seen in a separate high resolution set-up greater than 114 lines/mm in BaTiO₃ by itself.) The imaging geometry used for these preliminary demonstrations is not optimized, and further work will be done with considerable improvement expected. In addition, effects such as damping of the higher order modes relative to the lower order modes (which could cause a scrambling or loss of information) and polarization scrambling effects will be examined. In the latter case typical commercial fibers do not preserve polarization. Hence the linearly polarized input probe beam will emerge randomly polarized. For our DFWM experiments the pumps are linearly polarized in the plane of the experiment and only this component of polarization is conjugated.

Because of the possible systems applications it was of interest to see if a fiber could be used as the nonlinear medium itself. The experimental arrangement for the DFWM experiments using fused silica fibers as the phase conjugate medium is shown in Figure 7. The forward pump and probe were brought in parallel to each other and were symmetrically displaced from the optic axis of the first lens. This lens was designed to couple the forward pump and probe into the low order modes of the fiber. The backward pump was coupled into the other end of the fiber by a microscope objective. The backward pump was also aligned to launch only low order modes. The fibers used were typically 5 m in length and have been discussed earlier.

In performing these tests we encountered difficulties in determining if, in fact, a DFWM signal was observed because of signal-to-noise problems fundamental to a DFWM experiment in fibers. There are two basic noise sources, one arising from the backward traveling pump and the other due to Fresnel reflection of the probe from the input end of the fiber. Both signals limit the DFWM reflectivity that can be detected and are larger than the expected signal based on a simple calculation (see below). To understand these noise sources refer to Figure 7. The experimental arrangement allowed us in principle to spatially separate the forward pump, backward pump and probe. The signal was separated from the probe path by the signal-beam splitter. The problem was to launch only the lowest order modes. For best coupling it was necessary for the forward pump and probe to be physically collinear with the optic axis of the first lens. But for good phase conjugate signal separation the probe should be as far from the optic axis as physically possible, i.e., as close to the edge of the lens aperture as

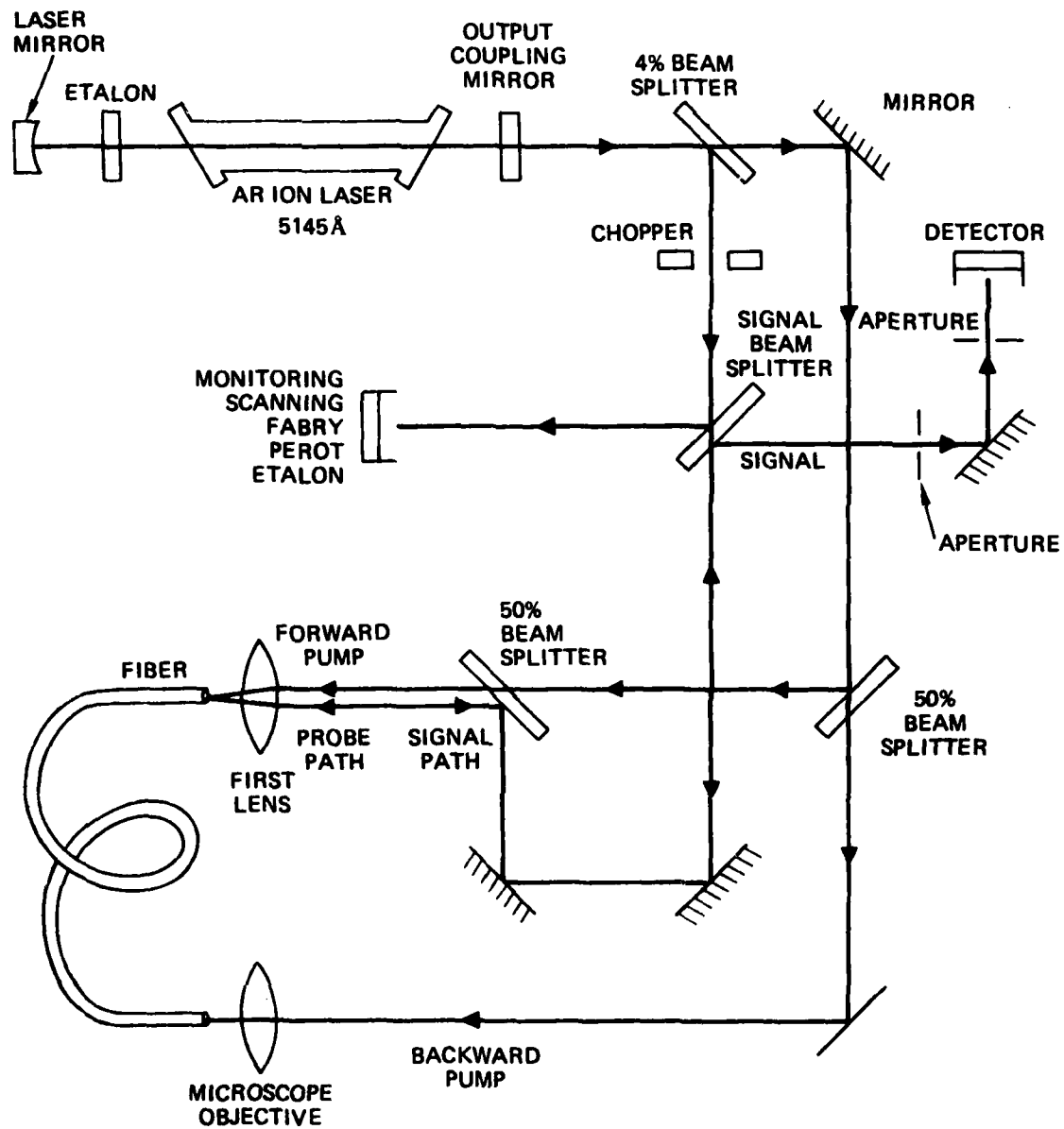


Figure 7. Schematic of degenerate four wave mixing experiments using silica fiber as nonlinear medium.

possible. In our preliminary work we attempted a compromise between these conditions. Unfortunately, because of mode coupling in the fiber there was enough energy coupled from the backward pump into higher order modes that the energy in these modes traveled back the same path as the signal. Phase lock detection was used (while chopping the probe), but the scattered backward pump prevented a conclusive measurement. The second source was the probe retro-reflection off the end of the fiber and coupling optics. We were able to reduce this retro-reflection by incorporating a polarizer-quarter wave plate combination. The linearly polarized light from the polarizer passed through the $\lambda/4$ plate at 45° with respect to the ordinary and extraordinary axis. The emergent light was then circularly polarized and impinged on the fiber end. The reflected light was also circularly polarized. The light then retraversed the $\lambda/4$ plate and emerged linearly polarized but now perpendicular to the input polarization and was attenuated by the polarizer. The signal polarization is not preserved in the fiber and emerged with a random polarization and the component parallel to the polarizer was passed. Even with this solution to the retro-reflection problem, we were unable to detect a DFWM signal, which is not surprising if one does a simple calculation of the expected conjugate signal strength, as given below.

For a nonresonant material the phase conjugate reflectivity is given by

$$R = \tan^2 |K| l \quad , \quad (5)$$

where

$$|K| \text{ (cm}^{-1}\text{)} = \left(32 \times 10^7 \frac{\pi^3}{c} \right) \frac{\chi^{(3)} \text{ (esu)}}{\lambda \text{ (cm)} n^2} \sqrt{I_1 I_2 \text{ (w/cm}^2\text{)}} \quad (6)$$

For silica glass the linear and nonlinear indices of refraction are:

$$n_0 = 1.5$$

and

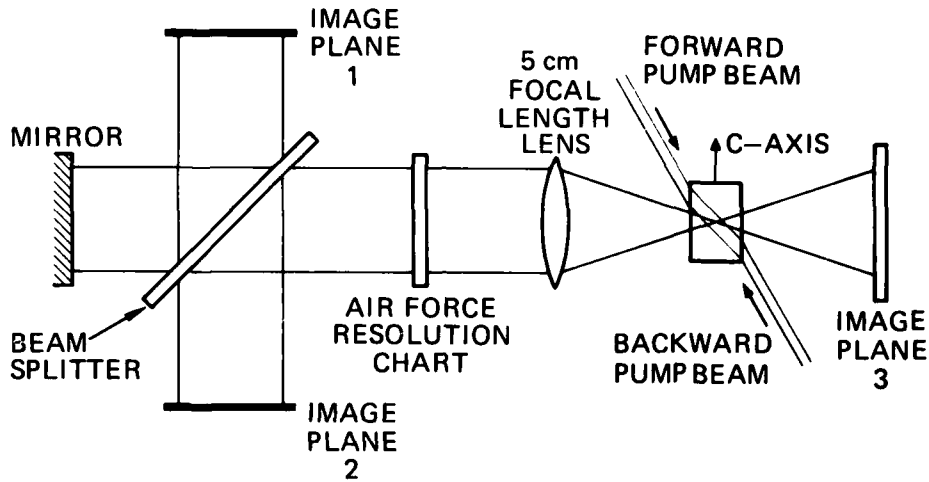
$$n_2 = 1.8 \times 10^{-13} \text{ esu,}$$

giving

$$\chi = \frac{n_2 n_0}{2\pi} = 4.3 \times 10^{-14} \text{ esu .}$$

For fiber diameters of 100 μm and for an input power of 1 W, $I = 2 \times 10^2$. Thus for a wavelength of 0.5 μm and a fiber length of 100 cm, $R = 10^{-5}\%$. In order to increase this reflectivity one could dope the fiber, thus increasing the nonlinear susceptibility.

As a result of the large phase conjugate returns obtained in BaTiO_3 , we performed a separate experiment to see if image amplification could be achieved using a phase conjugate oscillator configuration. These experiments were done on an AFOSR contract (F49620-80-C-0041) and are included here due to their relevance to this program. The resonator consisted of a phase conjugate mirror and a conventional mirror, shown in Figure 8(a). The oscillation occurs when noise between the mirror is amplified by energy supplied from the pump waves. With the onset of oscillation we have observed significant pump depletion. Typical operating parameters were $\sim 30 \text{ mW}$ out of the oscillator with $\sim 30 \text{ mW}$ in each of the pump beams. This resonator is unique because one can readily place two dimensional patterns in the cavity without destroying the oscillation. To illustrate this, an Air Force resolution target was placed within the cavity. Because the light exactly retraces itself after one cavity pass, the resolution chart test pattern is impressed on the output and image amplification occurs. The output from the oscillator in this configuration is shown in Figure 8(b).



(a)

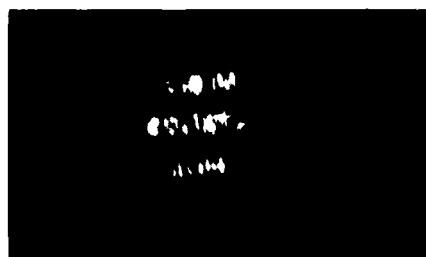


IMAGE AMPLIFICATION
OF AIR FORCE
RESOLUTION CHART
AT OUPUT OF
PHASE CONJUGATE
RESONATOR

(b)

Figure 8. (a) Phase conjugate oscillator configuration.
(b) Output at image plane 3 from phase conjugate oscillator with
Air Force Resolution chart in cavity.

SECTION 3

CONCLUSIONS

In the first year of this program we have analyzed photorefractive materials for phase conjugation of spatially modulated beams, and we have studied the use of phase conjugation for restoring images transmitted through multimode fibers. We have developed a detailed model of the photorefractive effect which will be used as a basis for comparing photorefractive materials for nonlinear phase conjugation. The results of the model highlight the importance of characterizing the impurities involved, and determining material parameters such as the electron mobility and cross sections associated with the impurity sites. One element of our program of study for the coming year will be an effort to measure or estimate such required parameters.

Our survey of mechanisms for DFWM (Table 1) has highlighted several nonlinear effects (aside from the photorefractive effect) with desirable properties for phase conjugation of spatially modulated optical signals. We plan to analyze and evaluate experimentally several of these techniques in the coming year.

We have successfully demonstrated the use of phase conjugation for restoring images transmitted through a 1.75 m multimode fiber. Preliminary results indicate that a resolution of 5 lines/mm was obtained, compared with a resolution without the fiber of ~20 lines/mm. We are devoting considerable attention to the characterization and optimization of our imaging optics. We expect considerable improvement in resolution in the near future.

REFERENCES

1. J.J. Amodei, RCA Review 32, 185 (1971).
2. N.V. Kukhtarev, V.B. Markov, S.G. Odulov, M.S. Soskin and V.L. Vinetskii, Ferroelectrics 22, 949 (1979).
3. J. Feinberg and R.W. Hellwarth, Opt. Lett. 5, 519 (1980).

APPENDIX A

PRELIMINARY REPORT ON THE MATHEMATICS OF PHOTOREFRACTIVITY

M. Sparks
Scientific Research Center
Santa Monica, CA 90401

RHr 8123

16 October 1981

Prepared for
Hughes Research Laboratories
3011 Malibu Canyon Road
Malibu, California 90265

TABLE OF CONTENTS

SECTION		PAGE
1	INTRODUCTION	A-1
2	MODEL OF PHOTOREFRACTIVITY	A-7
3	APPLIED-FIELD DOMINATED	A-15
4	DIFFUSION DOMINATED	A-27
5	PHOTOVOLTAIC-EFFECT DOMINATED	A-33
6	DEPLETION AND SATURATION	A-37
7	STEADY-STATE RESULTS	A-41
8	RESULTS OF KUKHTAREV AND COWORKERS AND OF AMODEI	A-49
9	PHOTOVOLTAIC EFFECT	A-55
10	MODEL OF DIELECTRIC RELAXATION	A-61
11	SUMMARY OF RESULTS	A-65
	REFERENCES	A-69

LIST OF ILLUSTRATIONS

FIGURE		PAGE
1	Schematic illustration of the photorefractivity model show in the various electronic levels in the bandgap	A-8
2	Schematic illustration of the positive and negative charge distributions for the case of short diffusion distance ($\Lambda k_g \ll 1$) showing the total charge distribution ρ that is spatially phase shifted with respect to the irradiance	A-19
3	Schematic illustration of the positive and negative charge distributions for the case of long diffusion distance ($\Lambda k_g \gg 1$) showing the total charge distributions ρ that is spatially in phase with the irradiance	A-24
4	Model for the photoelectric effect showing the idealized charge distribution resulting from net electron emission in the positive z direction	A-58
5	Crystal with an applied field with open-circuit conditions at the faces of the crystal showing the current density J, electric field E, and charged faces of the crystal.	A-62

ABSTRACT

A preliminary analysis of photorefractivity that will be used to understand the effect, interpret experimental results, plus select and improve materials and device performance is presented. Electron transport by diffusion, drift in an electric field, and the photovoltaic effect are considered both individually and collectively. Steady-state and short-time results are derived. Simple intuitive explanations of the response time, sensitivity, and spatial phase of the photorefractive electric field are given. The response time for writing and reading a grating is shown to be the dielectric-relaxation time when rewriting a new grating is neglected. The time response of lithium niobate can be improved by reduction, which increases the ratio of the densities of filled (Fe^{2+}) to empty (Fe^{3+}) levels.

APPENDIX A

SECTION 1

INTRODUCTION

The purpose of this study of photorefractive materials is to develop a theory of photorefractivity, with emphasis on simple physical explanations of the results, in order to interpret experimental results, suggest experiments to be performed, identify materials parameters that should be measured, select and rate types of materials and specific material, and seek improved performance. Photorefractivity, which is the change in the refractive index of a material with irradiance, is analogous to photoconductivity, which is the change in the conductivity of a material with irradiance. A related effect, the photovoltaic effect, is the generation of a voltage by irradiance.

This interim report was prepared in order to make the mathematical details of the treatment of photorefractivity available at the earliest possible time and to solicit comments on the analysis. The details of the mathematical treatment of a simple photorefractivity model that we believe contains the essential fractures required to explain photorefractivity in LiNbO_3 , KNbO_3 , BaTiO_3 , and BSO ($\text{Bi}_{12}\text{SiO}_{20}$) are presented. The results of the present report will be applied to these materials, and others of current interest in a subsequent report. The emphasis to date has been on lithium niobate (LiNbO_3) because there is more information available on this material than on other materials, some of which may be better candidates for the intended applications. This information is useful in establishing the validity of the theory, which will be done to the extent possible before applying the theory as discussed above.

In a subsequent report, the speed and sensitivity of the various materials will be estimated, tables of values of material parameters will be compiled, materials will be compared, and methods of improving the performance will be discussed along with the effects of changing various system parameters. An important feature of the subsequent report will be a table establishing the operating regime for various materials under diverse operating conditions. Table 1 lists the various limits of laser-pulse

duration, electron-transport distance, and electron-transport mechanism. Finally, the present results will be related to previous results in the literature.

As an example of improving performance, the most important method for increasing the speed of lithium niobate is to reduce (the opposite of oxidizing) the sample, which increases the ratio of the densities of "filled" (N_{e0} , for Fe^{2+}) to "empty" (N_{+0} , for Fe^{3+}) levels. This ratio N_{e0}/N_{+0} , not the individual values of N_{e0} , determines the writing- and erasing-speed (for fairly wide ranges of values of N_{e0} and N_{+0}), as seen in the expression for the dielectric-relaxation frequency in Equation 3.7.

The dielectric-relaxation frequency determines the write- and erase-times. (Rewriting a new grating during erasure is known to affect the erase time.) There are several characteristic times in the photorefractive effect including the following: the recombination time of electrons and empty optical-donor levels, the characteristic time for the irradiance to generate free carriers, the dielectric relaxation frequency, the trapping time, and the thermal freeing time. The time constant that controls the writing and erasing times is the dielectric relaxation frequency for all cases, namely, diffusion-, applied-field-, and photo-voltaic effect-controlled. It is important to use the correct carrier density, which is the carrier density generated by the write-or erase-beams, in the dielectric relaxation frequency. It is assumed for now that the explanation of the difference between write- and erase-times and between erase times for different c-axis directions is that the writing of a "secondary grating" by the erase- and diffracted-beams is correct. This effect will be investigated in a later report.

Table 1. Operating Conditions and Material Parameters

Laser-Pulse Duration, t	Short-Time $t \ll \tau_{d1}$		Steady-State $t \gg \tau_{d1}$
Electron-Transport Distance, Λ	Short-Transport $\Lambda k_g \ll 1$		Long-Transport $\Lambda k_g \gg 1$
Electron-Transport Mechanism	Diffusion	Applied Field	Photovoltaic Effect

The dielectric frequency given by Equation 3.7, the result for the space charge electric field E that gives rise to the grating, and the relation for the grating efficiency for a given E determine the performance of the photorefractive material. This grating electric field is not to be confused with the electric field of the optical beams. The response time, which is the read-or write-time in the absence of writing a secondary grating during erasure is independent of the grating wave vector k_g and diffusion distance Λ . By contrast, the electric field E depends on Λ and k_g in general.

The photorefractive effect is as follows: Illuminating a material with light generates free carriers, which are assumed to be conduction electrons for simplicity in the present treatment. Holes can contribute to the photorefractive effect in general, but are often negligible. The conduction electrons are assumed to come from such impurity levels in the electronic band gap as Fe^{2+} levels in $LiNbO_3$, but could, in general, come from direct excitation of electrons across the gap, by one- or two-photon absorption, for example. These impurity levels will be called optical-donor levels. The electrons drift, if they experience an electric field or diffuse to a new location in the crystal where they recombine with empty optical-donor levels. The space-charge electric field generated between the electrons in their new positions and the empty, positively charged optical-donor levels which remain in their original positions causes the refractive index to change by the electro-optic effect.

In addition to drift in an externally applied dc field and diffusion, the photovoltaic effect can contribute to the photoinduced electric field E . The components of E resulting from diffusion, E_d , drift in the net electric field ($E + E_{app}$, where E_{app} is an externally applied field assumed to be spatially constant), E_{dr} , and the photovoltaic field, E_p ,

$$E = E_d + E_{dr} + E_p$$

are discussed below. A typical value of E is 10^4 V/cm. The resulting change in the refractive index, which is called the grating index, is

$$n_g = \frac{1}{2} n_r^3 rE, \quad (1.1)$$

where n_r is the refractive index and r is the appropriate linear electro-optic coefficient, having a typical value of 10^{-8} cm/V, which gives $n_g \approx 0.5 (2.3)^3 10^{-8} 10^4 = 6 \times 10^{-4}$

In such optical processing as four-wave mixing used for phase conjugation, the irradiance changes from one position to another in the crystal. For example, the beat patterns of two overlapping beams causes a periodic irradiance. To be concrete, we assume a sinusoidal irradiance distribution for writing a grating

$$I = \langle I \rangle (1 + M \cos k_g z) \quad (1.2)$$

where $\langle \rangle$ denotes the spatial average

$$\langle I \rangle = \frac{1}{L} \int_0^L dz I \quad (1.3)$$

and

$$k_g = 4\pi n_r \sin \theta / \lambda, \quad (1.4)$$

with 2θ the full angle in the material between the direction of propagation of the two beams, λ is the wavelength of the light in vacuum, and λ/n_r is the wavelength of the light in the material.

The electric field and the resulting index of refraction n_g have a spatial frequency component at the grating wavelength k_g . This index grating can diffract an incoming light beam with efficiency¹ (for a thick grating)

$$\eta = e^{-\alpha d / \cos \theta} \sin^2 \frac{\pi n_r n_g d}{2 \lambda \cos \theta}, \quad (1.5)$$

where α is the optical absorption coefficient, d is the thickness of the sample, 2θ is the full angle between the two writing beams, n_r is the index of refraction of the material, n_g is the change in the index resulting from the photorefractive effect, and λ is the vacuum wavelength of the writing beams.

There is general agreement in the literature that this description of the photorefractive effect is correct. However, there is disagreement as to such details of the model as which electron transport mechanisms — drift, diffusion, or asymmetric photogeneration of electrons (photovoltaic effect) — is operative in a given material and why the grating efficiency increases or decreases with increasing pulse duration t_p for a given energy density It_p , rather than remaining constant as predicted by early theories.

The model is discussed in Section 2. In order to make the first analysis as simple as possible, the first case considered (see Section 3) is that of an applied field only. Diffusion, the photovoltaic effect, depletion, and saturation are neglected. The case of diffusion only and of photovoltaic only are considered in Sections 4 and 5 respectively in order to determine the effects of these two transport processes acting individually. Depletion and saturation are considered in Section 6. The steady-state grating electric field with an applied electric field, diffusion, and the photoelectric field included is derived in Section 7. The results of Kukhtarev and coworkers² and of Amodei³ are related to the present work and discrepancies between the three sets of results are resolved in Section 8. Simple pedantic models of the photovoltaic effect and of dielectric relaxation are given in Sections 9 and 10. A summary of the mathematical results are given in Section 11. The Appendix contains a list of symbols and typical values of parameters for lithium niobate.

Electrostatic units (esu) are used in the equations. Numerical results are given in both electrostatic units and rationalized mks units. Conversion factors are listed in the Appendix for the convenience of the reader.

Important results are denoted by underscored equation numbers and used in the summary (Section 11).

SECTION 2

MODEL OF PHOTOREFRACTIVITY

The analysis of even the simplest model of photorefractivity is complicated when carried out without approximations because the coupled material's equations and Maxwell's equations are nonlinear, coupled, partial differential equations. In order to develop the physical understanding required for materials-improvement programs and operation-improvement programs, a simple model is discussed first, then the effects of the assumptions made in the simple model are discussed.

The simplest model of photorefractivity is as follows: The material is an insulator with N_D optical levels per cubic centimeter in the electronic bandgap. See Figure 1. The levels are sufficiently deep that they are not thermally excited into the conduction band. The levels are called optical-donor levels because electrons from these levels are photoexcited into the conduction band. The density of the optical-donor levels that are filled with electrons is N_e and the density that are unfilled is N_+ . For example, N_e could be the Fe^{2+} density in lithium niobate, N_+ and Fe^{3+} density, and $N_D = N_e + N_+$ the total iron density including both Fe^{2+} and Fe^{3+} . In general, there are many filled levels N_e and many empty levels N_+ . The ratio N_e/N_+ can be varied by oxidizing or reducing the sample or by doping with compensating impurities. In order to make the crystal have charge neutrality, there must be negative impurities or imperfections present to compensate for the positive charges of the iron. The density of these levels that compensate for the extra positive charge of the Fe^{3+} is equal to the value N_{+0} of N_+ before the irradiance is turned on. Subscript zeros denote the values of parameters at $t = 0$, i.e., the time at which the irradiance is turned on.

Holes are neglected for simplicity. Electrons are generated from the filled optical-donor levels to the conduction band by the irradiance and recombine with empty optical-donor levels. Trapping is neglected in this first model. We used the common photoconductivity terminology that electrons in traps can be thermally re-excited into the conduction band. Thus, the capture of electrons by the empty optical-donor levels is called recombination, rather than trapping. This recombination into the optical-donor levels is not to be confused with recombination of holes and electrons across the gap.

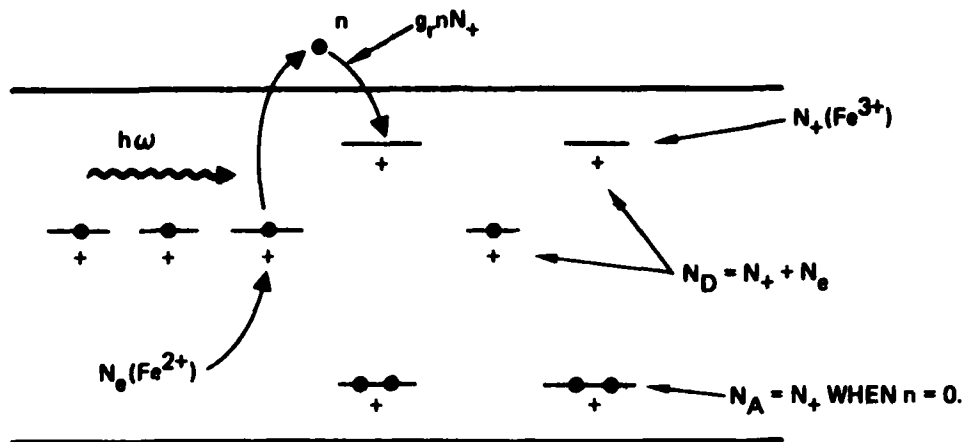


Figure 1. Schematic illustration of the photorefractivity model show the various electronic levels in the bandgap.

Saturation and depletion of the optical-donor levels are neglected when possible. However, they must be included in the analysis of the steady state because the correct steady state is not attained in general when saturation and depletion are neglected.

The simple model is believed to be sufficient to explain the performance of iron-doped lithium niobate, and it may be sufficient for the other materials of current interest. Extensions of the model and the applicability to other materials will be considered in subsequent studies and reports.

The number of electrons per cubic centimeter generated by the light is equal to the number of photons per cubic centimeter absorbed, which is equal to the absorbed energy per cubic centimeter, αI , (where α is the optical absorption coefficient) divided by the photon energy $h\omega$:

$$(\partial n / \partial t)_I = (\partial N_+ / \partial E)_I = \alpha I / h\omega .$$

It was assumed that one free electron is generated for every absorbed photon. This generation rate can be written in several convenient forms as follows:

$$\alpha I / h\omega = \sigma_D N_e / h\omega = \gamma_I N_e = \langle \gamma_I \rangle N_e (1 + M \cos k_z z) , \quad (2.1)$$

where Equation 1.2 was used for I and

$$\alpha = \sigma_D N_e , \quad (2.2)$$

$$\gamma_I = \sigma_D I / h\omega , \quad \langle \gamma_I \rangle = \sigma_D \langle I \rangle / h\omega \quad (2.3)$$

where σ_D is the optical absorption cross section of the optical donor levels.

The change in the electron concentration resulting from movement of the electrons away from the generation region (and from the motion of the electrons in general) is described by the charge continuity equation:

$$\partial\rho/\partial t = \nabla \cdot \underline{J} = -dJ/dz \quad (2.4)$$

where the charge density is

$$\rho = e(N_+ - N_{+0} - n) = e(N_{+\Delta} - n) \quad (2.5)$$

where $e = |e|$, the absolute magnitude of the electron charge; $N_{+\Delta} \equiv N_+ - N_{+0}$; and J is the electrical current ($-e$ times the net rate at which electrons cross a unit area of surface). Substituting Equation 2.5 into Equation 2.4 gives the first central equation — Equation 2.8 below. The recombination rate is

$$(\partial n/\partial t)_{\text{recomb}} = -v_{\text{th}} s N_+ n$$

where the recombination frequency is

$$\gamma_r = v_{\text{th}} s N_{+0} \quad (2.6)$$

where s is the cross section for the capture of an electron by an empty optical donor level (having density N_+), and v_{th} is the average thermal velocity of the electrons, which has the value:

$$v_{th} \cong 10^7 \text{ cm/sec} \quad (2.7)$$

at room temperature. Combining these contributions gives the basic equations:

$$\partial n / \partial t = \partial N_+ / \partial t + e^{-1} dJ/dz \quad (2.8)$$

$$\partial N_+ / \partial t = -\partial N_e / \partial t = \gamma_I N_e - \gamma_r n N_+ / N_{+0} \quad (2.9)$$

$$J = -e\mu n E + eD \partial n / \partial z + \rho N_e \hat{c} \quad (2.10)$$

$$\partial E / \partial z = 4 \frac{\hat{c}}{wE}^{-1} \rho \quad (2.11)$$

$$\rho = e(N_+ - N_{+0} - n) = e(N_{+\Delta} - n) \quad (2.12)$$

$$E = E_{app} + E_{sc} \quad (2.13)$$

where D is the diffusion coefficient, ρ is the photovoltaic coefficient, \hat{c} is the unit vector along the photovoltaic direction, and $e = |e|$. The contributions to the current in Equation 2.10 are as follows: $-e\mu n E \cong -eV_{drift} n$ is the

usual electrical-conductivity current $J = \sigma E$; $eD\partial n/\partial z$ is the diffusion current; and $pN_e I_c^A$ is the photovoltaic current, as discussed in Section 9.

These system Equations 2.8 through 2.13 are nonlinear because they contain products N_+n and nE (where E is a function of n and N_+). Thus, their solution is nontrivial, and the complexity of the general results would obscure simple interpretation. The following limiting cases will therefore be considered:

- (a) $k_g \Lambda \ll 1$ and $k_g \Lambda \gg 1$
- (b) drift, diffusion, and photovoltaic-effect-dominated
- (c) short-time limit and steady state,

where Λ is the electron-transport distance, as discussed below.

For all cases, a first approximation which will be relaxed below for special cases, the equations are linearized by neglecting depletion and saturation. Depletion is the reduction in the absorption coefficient α resulting from depletion of the electrons in the optical-donor levels, and saturation is the reduction in the recombination rate γ_r resulting from filling of the recombination levels (which are the empty optical-donor levels N_+ in the present model) with electrons. Depletion is negligible when $N_e \cong N_{e0}$, and saturation is negligible when $N_+ \cong N_{+0}$. To be more specific, define the changes $N_{+\Delta}$ and $N_{e\Delta}$ as

$$N_{+\Delta} \equiv N_+ - N_{+0} \quad (2.14)$$

and

$$N_{e\Delta} \equiv N_e - N_{e0} \quad (2.15)$$

Since $\partial N_e / \partial t = -\partial N_+ / \partial t$ according to Equation 2.9

$$N_{+\Delta} = -N_{e\Delta} \quad , \quad (2.16)$$

Thus, the approximations of negligible depletion and saturation are, respectively,

$$|N_{+\Delta}| \ll N_{+0} \quad , \quad (2.17)$$

$$|N_{e\Delta}| = |N_{+\Delta}| \ll N_{e0} \quad . \quad (2.18)$$

For negligible saturation, the optical absorption coefficient $\alpha = \sigma_D N_e$ is constant. Thus,

$$\alpha = \sigma_D N_{e0} \quad , \quad \text{for negligible depletion.} \quad (2.19)$$

For negligible saturation, the recombination frequency $\nu_{th} s N_+$ is constant. thus

$$\gamma_r = \nu_{th} s N_{+0} \quad , \quad \text{for negligible saturation.} \quad (2-20)$$

SECTION 3

APPLIED-FIELD DOMINATED

In this section, diffusion, the photovoltaic effect, depletion, and saturation are neglected. The electron-drift distance is

$$\Lambda_E = \mu \tau_r E ,$$

where $\tau_r \equiv 1/\gamma_r$ is the recombination time and μE is the drift velocity. The two limits of short drift distance, $k_g \Lambda_{dr} \ll 1$ and long drift distance $k_g \Lambda_E \gg 1$, will be considered.

The steady-state solution of Equation 2.9 with $N_e \equiv N_{e0}$ and $N_+ \equiv N_{+0}$ is

$$n = (\gamma_I / \gamma_r) N_{e0} = \langle n \rangle (1 + M \cos k_g z) \quad (3.1)$$

where

$$\langle n \rangle = (\langle \gamma_I \rangle / \gamma_r) N_{e0} . \quad (3.2)$$

typical value

$$\tau_r = 1/v_{th} s N_{+0} = 0.2 \text{ ns}/c_+ (\text{ppm}) = 20 \text{ psec} \quad (3.3)$$

for $v_{th} = 10^7$ cm/sec (at room temperature), electron-ion cross section for a changed recombination center $s = 10^{-14}$ cm², and recombination center density $N_{+0} = 5 \times 10^{17}$ cm⁻³ for a lightly doped sample with concentration $c_+ = N_{+0}/N_{atomic\ sites} = 10$ ppm. For heavily doped samples, τ_r is even shorter than the value of 20 psec in Equation 3.3. Thus, for pulse durations and doping concentrations of current interest, $\tau_r \ll t$ is satisfied throughout most of the pulse duration. Furthermore, n is given by the steady-state value in Equation 3.1, except at very short times which will be neglected here. Physically, for negligible electron drift distance, the electrons are trapped where they are generated. Thus, setting $J = 0$ in Equation 2.10 as a zeroth-order approximation and solving for n gives an exponential rise to the value in Equation 3.1 with rise time τ_r .

Having calculated n under the zeroth-order approximation, $J = 0$, this value of n and the nonzero value of $J = -e\mu nE$ in the next-order approximation cause N_+ to continue to change after n has reached its steady state. For short times (i.e., before the space charge field E_{sc} builds up to substantially change the electric field in Equation 2.9 from its original value $E_0 = E_{app}$), Equation 2.10 gives:

$$J \cong J_0 = -e \mu n^2 E_{app} .$$

Substituting this J into Equation 2.4 and integrating over time, with $\rho = \rho_0 = 0$ at $t = 0$, gives

$$\rho = -e\mu \langle n \rangle E_{app} \frac{k M t \sin k z}{g} . \quad (3.4)$$

The space-charge electric field resulting from the charge distribution in Equation 3.4, obtained by integrating Poissons equation

$$\nabla \cdot \underline{D} \cong \epsilon \partial E / \partial z = 4 \pi \rho \quad (3.5)$$

is

$$E_{sc} = \gamma_{di} t E_{app} M \cos k_g z \quad (3.6)$$

where the dielectric relaxation frequency is

$$\gamma_{di} = 4 \pi \sigma / \epsilon = 4 \pi e \mu \langle n \rangle / \epsilon = 4 \pi e \mu \sigma_D \langle I \rangle N_{e0} / e h \omega_{th} N_{+0} \quad (3.7)$$

One of the important results of the present study is that the response time (the read- and write-time in the absence of writing of a secondary grating) is the dielectric relaxation time $\tau_d = 1/\gamma_{di}$. Consideration of the expression for γ_{di} in Equation 3.7 can lead to estimates of the response time and to suggestions on how to increase the speed, as discussed briefly in Section 1. This electric field is in spatial phase ($E \sim \cos k_g z$) with the irradiance, in agreement with the results obtained below by physical arguments.

It is instructive to rederive this electric-field distribution in Equation 3.5 by physical argument in order to gain intuition. Once the steady state value of n is attained, electrons that are generated at z by the irradiance are trapped at $z + \lambda_g$ on the average. The trapped-charge density $e_{N+\Delta}$ (see Equation 2.12) can therefore be written as the sum of two terms, a positive term from the N_+ at z where an electron is generated and a negative term of equal absolute magnitude but displaced by distance λ_g , corresponding to the recombination of the electron at $z + \lambda_g$. In other words, the

current causes a buildup of the displaced trapped electrons and a corresponding build up of the positive charges left behind (see Figure 2). Integrating the generation equation $(\partial N_+ / \partial t)_{\text{gen}} = (\partial N_{+\Delta} / \partial t)_{\text{gen}} = \gamma_I N_{e0}$ for short times gives

$$(eN_{+\Delta})_{\text{gen}} = e \langle \gamma_I \rangle N_{e0} t (1 + M \cos k_g z) \quad . \quad (3.8)$$

The corresponding negative, displaced, recombination term is

$$(eN_{+\Delta})_{\text{rcmb}} = -e \langle \gamma_I \rangle N_{e0} t [1 + M \cos k_g (z - \Lambda_{dr})] \quad . \quad (3.9)$$

Adding these two terms and using the Taylor expansion $\cos k_g (z - \Lambda_E) \cong \cos k_g z + \Lambda_E k_g \sin k_g z$ gives

$$eN_{+\Delta} = -e \langle \gamma_I \rangle k_g \Lambda_E N_{e0} t M \cos k_g z \quad . \quad (3.10)$$

With $\rho \cong eN_{+\Delta}$ and $\langle n \rangle = (\langle \gamma_I \rangle / \gamma_r) N_{e0}$, Equation 3.10 gives Equation 3.4. The rest of the derivation of the space-charge field resulting in Equation 3.6 is the same as above. The charge resulting from n and the corresponding $N_{+\Delta}$ is easily shown to be given by the ρ in Equation 3.4 times τ_r / t , which is negligible for $t \gg \tau_r$.

As the time increases, the space charge field E_{sc} continues to increase according to Equation 3.6 until it is no longer negligible. Then the approximation $E \cong E_{app}$ is no longer valid, and Equation 3.5 is no longer valid. The electric field for intermediate times is more difficult to calculate, but the steady-state value is again easy to calculate. In the steady-state, $\partial n / \partial t = 0$ and $\partial N_+ / \partial t = 0$; thus, Equation 2.8 gives $\partial J / \partial z = 0$, or

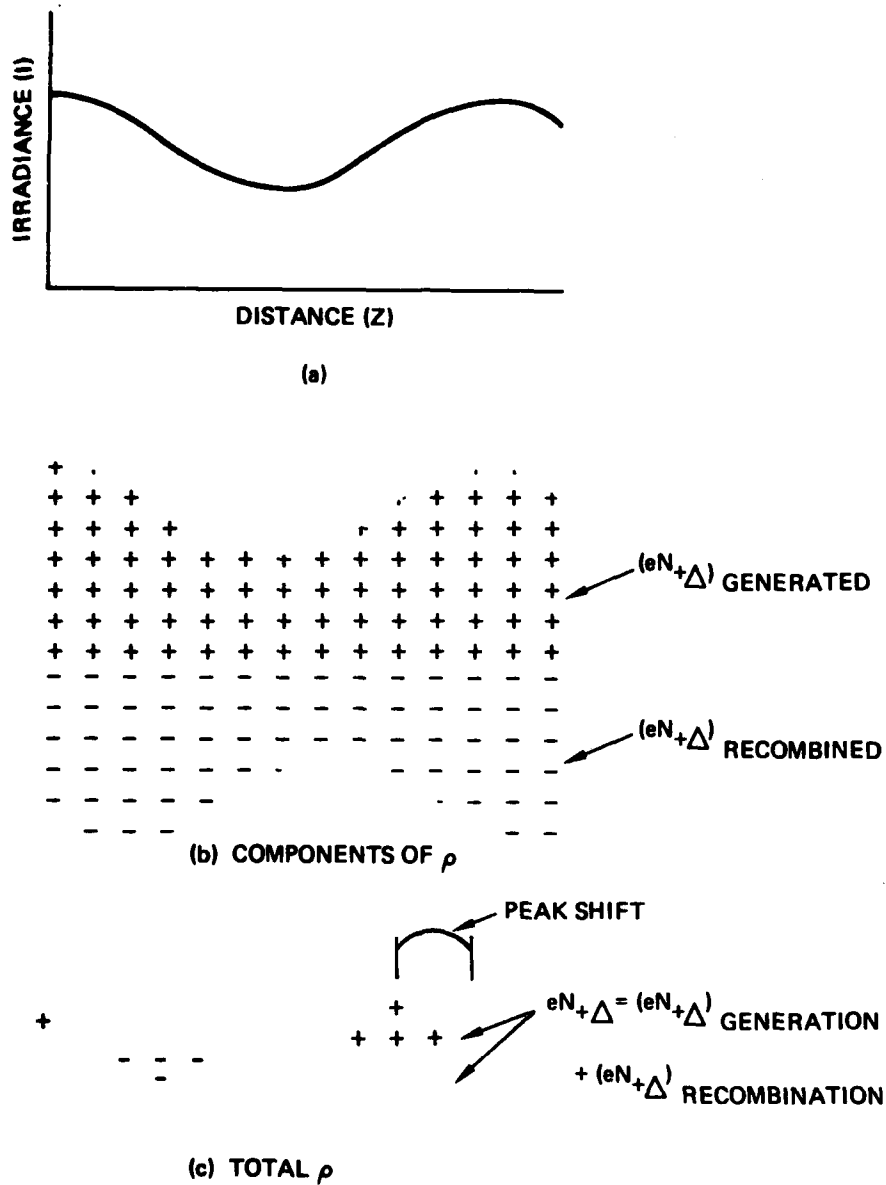


Figure 2. Schematic illustration of the positive and negative charge distributions for the case of short diffusion distance ($\Lambda k \gg 1$) showing the total charge distribution ρ that is spatially phase shifted with respect to the irradiance.

$$J = \text{constant} \equiv J_0 \quad .$$

For the present case of drift only, setting $D = \rho = 0$ in Equation 2.10 gives

$$J = -e\mu nE \quad . \quad (3.11)$$

From Equations 3.10, 3.2, and $J = J_0$,

$$E = -\frac{J_0}{e\mu n} = -\frac{J_0/e\mu \langle n \rangle}{1 + M \cos k_g z} \quad . \quad (3.12)$$

The divergence in E for $M = 1$ at $\cos k_g z = -1$ is unphysical. It arises from the assumption that the transport (drift) length is zero. For nonzero transport length, M is replaced by a number less than unity, as suggested by Amodei² and shown by Kukhtarev and coworkers.³ The field E is not sinusoidal except in the limit of $M \ll 1$ (where the expansion $(1 + M \cos k_g z)^{-1} \approx 1 + M \cos k_g z$ is valid).

An important feature of the field E (which gives rise to the grating) is obvious when E is expressed in terms of J_0 , as in Equation 3.12, although it has not been discussed previously to my knowledge. For open circuit conditions, the steady-state field E vanishes because $J_0 = 0$ (no current for an open circuit). In order to write a steady-state grating (i.e., have $E \neq 0$) in the steady-state with drift alone, there must be an external circuit through which a current can flow. Otherwise, the faces of the crystal are charged by the nonzero current before the steady-state is reached, and the current approaches zero as the time approaches infinity and the charges on the faces approach the value required to make $E_g = -E_{app}$ (i.e., $E = 0$). At intermediate times, the grating is nonzero.

A rough approximation to the full time dependence for this case (of $k_g \Lambda_{dr} \ll 1$, E_{app} dominated, negligible depletion and saturation, and $J = 0$) is obtained as follows: The charging of the faces of the crystal gives, from Appendix A:

$$E = E_{app} e^{-\gamma_{di} t} \quad , \quad (3.13)$$

where the dielectric relaxation frequency is given by Equation 3.7. Formally replacing $E = E_{app}$ in Equation 3.6 by E in Equation 3.13 and including the spatially constant space-charge field gives

$$E \cong e^{-\gamma_{di} t} (E_{app} + \gamma_{di} t E_{app} M \cos k_g z) \quad . \quad (3.14)$$

The maximum of the $\cos k_g z$ term occurs at

$$t = \tau_{di} \equiv 1/\gamma_{di} \quad (3.15)$$

and has the value (writing $\exp(-1)$ to avoid confusion with the electron charge):

$$E_{mx} = \exp(-1) E_{app} M \cos k_g z \quad . \quad (3.16)$$

Since the dielectric relaxation time is the time at which the steady-state is approached, as an approximation to the full time dependence, we multiply the short-time electric field $E_{\text{short-t}}$ by $\exp(-\gamma_{\text{di}}t)$ and add the result to $f^2 \equiv [1 - \exp(-\gamma_{\text{di}}t)]^2$ times the steady-state value E_{ss}

$$E \cong E_{\text{short-t}} e^{-\gamma_{\text{di}}t} + E_{\text{ss}} (1 - e^{-\gamma_{\text{di}}t})^2 \quad (3.17)$$

The square of f was used rather than f to insure that $E \cong E_{\text{short-t}}$ at short times. This approximation in Equation 3.17 does not correspond to an exact solution of the systems equation. It is simply an intuitive approximation to the full time dependence. It does give the correct short-time field and steady-state field, and it does develop with time constant $\tau_{\text{di}} = 1/\gamma_{\text{di}}$. The value of E at intermediate times may not be highly accurate.

With $E_{\text{short-t}}$ given by Equation 3.6 and E_{ss} given by Equation 3.12, substituting in Equation 3.17 gives

$$E \cong \gamma_{\text{di}} t e^{-\gamma_{\text{di}}t} E_{\text{app}} M \cos k_g z + [-(J_0/\epsilon\mu\langle n \rangle)/(1 + M \cos k_g z)] (1 - e^{-\gamma_{\text{di}}t})^2 \quad (3.18)$$

Next consider the case of $k_g \Lambda_{dr0} \gg 1$, where $\Lambda_{dr0} = \mu \tau_r E_{app}$. Since the electrons then drift a distance long with respect to the grating distance k_g^{-1} , the electron density is approximately constant spatially for $t > \tau_r$. Since the free-electron generation rate $(\partial n / \partial t)_{gen} = \gamma_I N_e$ and recombination rate $(\partial n / \partial t)_{rcmb} = \gamma_r n$ are the same as for the case of $k_g \Lambda_{dr} \ll 1$, the value of this constant n is just the average value of n from Equation 3.1

$$n \cong \langle n \rangle = (\langle \gamma_I \rangle / \gamma_r) N_{e0} \quad (3.19)$$

The recombination then occurs evenly over all z (rather than at a short distance from the generation region as was the case for $k_g \Lambda_{dr} \ll 1$). Figure 2 (for $k_g \Lambda_{dr} \ll 1$) is then replaced by Figure 3 for the case of $k_g \Lambda_{dr0} \gg 1$, and the second term in Equation 3.9 is replaced by zero, corresponding to spreading the charge $eN_{+\Delta c} \cos k_g(z - \Lambda_{dr})$ evenly throughout the crystal. The resulting value of $eN_{+\Delta} = (eN_{+\Delta})_{gen} + (eN_{+\Delta})_{rcmb}$ from Equation 3.8 and the modified Equation 3.9 is

$$eN_{+0} = e \langle \gamma_I \rangle N_{e0} M t \cos k_g z \quad (3.20)$$

With $\rho \cong eN_{+0}$ and Equation 3.5, this gives

$$E_{sc} = 4\pi e \langle \gamma_I \rangle N_{e0} (k_g \epsilon) t M \sin k_g z \quad (3.21)$$

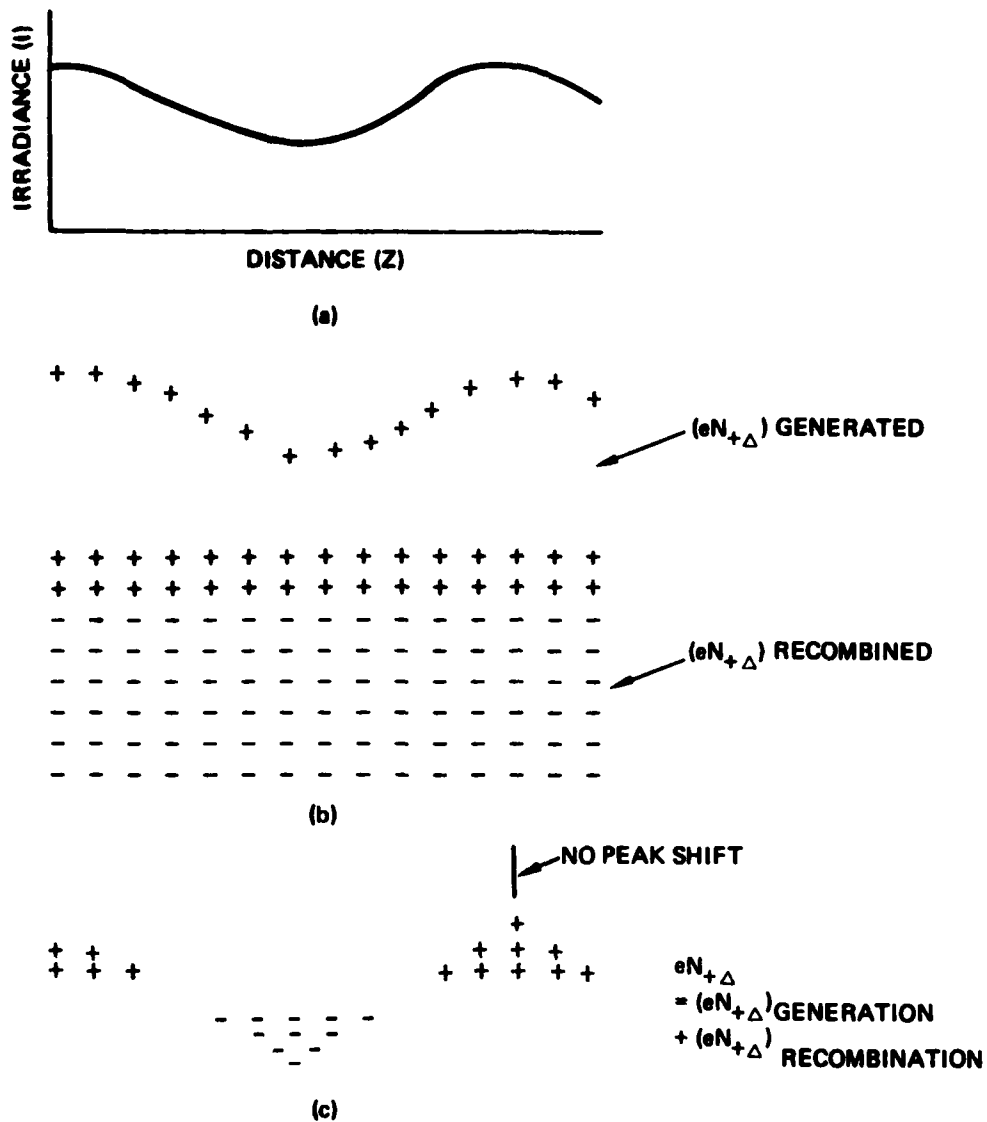


Figure 3. Schematic illustration of the positive and negative charge distributions for the case of long diffusion distance ($\Lambda k_g \gg 1$) showing the total charge distribution ρ that is spatially in phase with the irradiance.

which is written as

$$E_{sc} = \gamma_{df} t E_{\Lambda} \sin k_g z \quad (3.22)$$

where

$$E_{\Lambda} \equiv \gamma_r / \mu k_g \quad (3.23)$$

is the field at which the drift velocity μE_{Λ} is equal to k_g^{-1} / τ_r .

The steady-state value of E for arbitrary J_0 is, from Equation 3.11 and $J = J_0$,

$$E = -J_0 / e \gamma_r n \quad (3.25)$$

The corresponding steady-state value of the drift distance is

$$\Lambda_{Ess} = \mu E \tau_r = J_0 / e \gamma_r n \quad (3.26)$$

For $k_g \Lambda_{drss} \gg 1$, n is approximately constant as discussed above. Then Equation 3.25 gives $E = \text{constant}$; thus, there is no grating (which requires a z dependence of E) in this order of approximation. Keeping higher order terms in n gives a nonzero grating.

For $k_g \Lambda_{drss} \ll 1$, n is given by Equation 3.1 and there is a nonzero grating, which is given by Equation 3.26. Thus, Equation 3.25 gives the steady-state field

$$E = - \frac{J_0 / \epsilon \mu \langle n \rangle}{1 + a M \cos k_g z} \quad , \quad (3.27)$$

where

$$a = 1 \quad \text{for } J_0 k_g / e \gamma_r \ll 1$$

$$a = 0 \quad \text{for } J_0 k_g / e \gamma_r \gg 1 \quad .$$

Equations 3.17, 3.22, and 3.27 give

$$E \cong \gamma_{di} e^{-\gamma_{di} t} E_A M \sin k_g z - [(J_0 / \epsilon \mu \langle n \rangle) / (1 + a M \cos k_g z)] (1 - e^{-\gamma_{di} t})^2 \quad . \quad (3.28)$$

SECTION 4

DIFFUSION DOMINATED

As in the previous case of drift only, the charge density for the case of $k_g \Lambda_d \ll 1$ (where Λ_d is the diffusion distance discussed below) for diffusion only can be obtained from physical arguments similar to those used above in the discussion of Figure 3.1. For diffusion, half of the electrons diffuse to the left and half diffuse to the right, in contrast to the drift case above in which all electron drift to the right in Figure 2. Thus, Equation 3.9 is replaced by

$$\begin{aligned} (eN_{+\Delta})_{\text{rcmb}} = & -e\langle\gamma_I\rangle N_{e0} t \left[1 + \frac{1}{2} M \cos k_g (z - \Lambda_d) \right. \\ & \left. + \frac{1}{2} M \cos k_g (z + \Lambda_d) \right] . \end{aligned} \quad (4.1)$$

Using the Taylor expansion

$$\cos k_g (z \pm \Lambda_d) \cong \cos k_g z \pm k_g \Lambda_d \sin k_g z - \frac{1}{2} k_g^2 \Lambda_d^2 \cos k_g z$$

and adding Equations 4.1 and 3.8 gives

$$eN_{+\Delta} = \frac{1}{2} e\langle\gamma_I\rangle N_{e0} k_g^2 \Lambda_d^2 M t \cos k_g z . \quad (4.2)$$

With

$$\Lambda_d^2 = D\tau_r \quad (4.3)$$

where D is the diffusion coefficient. Using n given by Equations 3.1 and 3.2, Equation 4.2 and $\rho \equiv eN_{+\Delta}$ give

$$\rho \equiv \frac{1}{2} e D k_g^2 \langle n \rangle M t \cos k_g z \quad (4.4)$$

The corresponding electric field is, from Equation 3.5

$$E = E_{sc} = \frac{1}{2} \gamma_{di} t E_d M \sin k_g z \quad (4.5)$$

where

$$E \equiv D k_g / \mu \quad (4.6)$$

is the electric field for which the drift velocity μE_d is equal to the grating distance k_g^{-1} divided by the diffusion time $(D k_g^2)^{-1}$.

The steady-state value of E for the present case of $k_g \Lambda_d \ll 1$ and diffusion only is also easy to obtain. For diffusion only, the current, which must be spatially constant in the steady state, is zero, $J = J_0 = 0$, because there is no applied field and no surface charges. Setting $J = 0$ and $p = 0$ in Equation 2.10 gives

$$\mu n E = D \partial n / \partial z \quad . \quad (4.7)$$

Since $J = 0$, n is given by Equations 3.1 and 3.2. With Equation 4.7 this gives

$$E = \frac{E_d M \sin k_g z}{1 + M \cos k_g z} \quad (4.8)$$

For $M \ll 1$, $E \cong E_d M \sin k_g z$ is in spatial quadrature with the irradiance. When M is not small, E is not sinusoidal, just as it was not for the case of drift. By symmetry, the Fourier component in spatial phase is zero.

The electron transport stops when the drift in the space-charge field increases to the value at which this drift cancels the transport from diffusion. Thus, the characteristic time for the steady state to be approached is just the characteristic time for charge buildup, which is the dielectric-relaxation time $\tau_{di} = 1/\gamma_{di}$, where γ_{di} is defined in Equation 3.7. This time constant can be verified as follows: For convenience, set $\sin k_g z = 1$ and $\cos k_g z = 0$ in Equations 4.5 and 4.8. Equating the short-time solution in Equation 4.5 to the steady-state value in Equation 4.8 and solving for t gives one definition of the characteristic time (that would equal the exponential time constant if the E field increased exponentially). This gives $t = 2\tau_{di}$, which is approximately equal to the dielectric-relaxation time as expected.

From Equations 3.17, 4.5, and 4.8,

$$E \approx \gamma_{di} t e^{-\gamma_{di} t} \frac{1}{2} E_d M \sin k_g z + [E_d M \sin k_g z / (1 + M \cos k_g z)] (1 - e^{-\gamma_{di} t})^2 . \quad (4.9)$$

Next consider the case of $k_g \Lambda_d \gg 1$. In this long-diffusion-distance limit for short times, the electron density is constant and is given by Equation 3.17, just as for the case of $k_g \Lambda_{dr} \gg 1$ considered in Section 3. The electric field at short times is therefore given by Equation 3.20.

$$E = E_{sc} = \gamma_{di} t E_{rg} M \sin k_g z , \quad (4.10)$$

where

$$E_{rg} = \gamma_r / \mu k_g$$

as in Equation 3.21.

The steady-state value of E from Equation 4.7 with $n \cong \text{const}$ is $E = 0$. A nonzero value of E in the steady-state results from the next order correction to n . An example of the calculation of the steady-state value of E is given in Section 8 in the discussion of the results of Kukhtarev and coworkers.

From Equations 3.17 and 4.10

$$E \cong \gamma_{di} t e^{-\gamma_{di} t} E_{rg} M \sin k_g z + E_{Dss} (1 - e^{-\gamma_{di} t})^2 \quad . \quad (4.11)$$

As an example of E_{Dss} , from Section 8 for the case of $N_{+0} \ll N_{e0}$, from Equation 8.10

$$E_{Dss} = - (4\pi e N_{+0} / \epsilon k_g) M \sin k_g z \quad . \quad (4.12)$$

SECTION 5

PHOTOVOLTAIC-EFFECT DOMINATED

The photovoltaic effect is discussed in Section 9. It is easy to show that the results in Section 3 (for applied field only) are valid for the photoelectric effect if E_{app} is replaced by the steady-state photovoltaic field:

$$E_p = \Lambda_p \gamma_r / \mu = p N_e \langle I \rangle / e \mu \langle n \rangle \quad (5.1)$$

from Equation 9.8. This prescription of replacing E_{app} by E_p can be understood as follows: The central feature of the Glass⁵ explanation of the photovoltaic effect is that the electrons generated by the irradiance are emitted preferentially in a direction given by a unit vector \hat{c} . The electrons are displaced through an effective distance Λ_p in the \hat{c} direction, as discussed in Section 9. Thus, Equation 3.9 is valid if Λ_{dr} is replaced by Λ_p . The prescription of replacing E_{app} by E_p in the expression $\Lambda_{dr} = \mu E_{app} / \gamma_r$ is equivalent to replacing Λ_{dr} by Λ_p , as seen by making the replacement (5.1) in the Λ_{dr} expression. Replacing E_{app} by E_p in Equations 3.4 and 3.5 and integrating Equation 3.5 for short times gives, for $\Lambda_p k_g \ll 1$,

$$E \cong \gamma_{di} t E_p M \cos k_g z. \quad (5.2)$$

This result can also be obtained from the continuity equation $\partial p / \partial t = \partial J / \partial z$, with $I = -e \mu n E + p N_e I \cong p N_e I$ for short times. Notice that $k_g \Lambda_p \ll 1$ is always satisfied for cases of interest (because $\Lambda_p \cong 0.1$ nm and $k_g \cong 1/500$ nm).

As the time increases further, the space charge builds up until $J = J_0 =$ constant, which is the condition for the steady state as discussed above. Setting $J = J_0$ in Equation 2.10 (with $D = 0$), solving for the steady state field, and using

$$pN_{eo} \langle I \rangle / e\mu \langle n \rangle = \Lambda_p \gamma_r / \mu = E_p$$

gives

$$E = [E_p (1 + M \cos k_g z) - J_0 / e\mu \langle n \rangle] / (1 + M \cos k_g z). \quad (5.3)$$

The first term E_p is independent of z . Thus, there is no steady-state grating for open circuit conditions ($J_0 = 0$), just as for an applied field. However, there is a nonzero correction to this result when diffusion and/or an applied field are added. The $\langle n \rangle$ in the numerator in Equation 5.3, which comes from $n \cong \langle n \rangle (1 + M \cos k_g z)$ is a zeroth order approximation. Kukhtarev and coworkers obtained the following first order correction for the case of $k_g \Lambda \ll 1$:

$$n \cong \langle n \rangle [1 + M (1 - \xi) \cos k_g z] \quad (5.4)$$

where

$$\xi \equiv \xi_T + \xi_E = (E_d + E_{app})/E_g \quad (5.5)$$

with

$$E = 4\pi e N_{+0}/\epsilon k_g \quad (5.6)$$

Expanding in powers of ξ gives

$$\frac{1 + M \cos k_g z}{1 + M (1 - \xi) \cos k_g z} \cong 1 + \frac{\xi M \cos k_g z}{1 + M \cos k_g z}.$$

Thus, the z -dependent terms in Equation 5.3 for the case of $k_g \Lambda \ll 1$ are

$$E \cong (E_p \xi M \cos k_g z - J_0/e\mu\langle n \rangle)/(1 + M \cos k_g z). \quad (5.7)$$

[My preliminary results give a different correction to n from the value in Equation 5.4 by Kukhtarev and coworkers. The discrepancy, which is unimportant in the present cases, in which the photovoltaic effect is negligible, will be resolved in a later note.]

Combining Equations 3.17, 5.2, and 5.7 gives, for $\Lambda_p k_g \ll 1$,

$$E \cong \gamma_{di} t e^{-\gamma_{di} t} E_p M \cos k_g z \quad (5.8)$$

$$+ \frac{E_p \xi M \cos k_g z - J_0/e\mu\langle n \rangle}{(1 + M \cos k_g z)} (1 - e^{-\gamma_{di} t})^2, \text{ for } k_g \Lambda \gg 1$$

For E_{app} and D included and $K_g \Lambda \gg 1$, n is approximately constant. Then, replacing $1 + M \cos k_g z$ by 1 in the denominator in Equation 5.3 gives, for $k_g \Lambda \gg 1$

$$E \cong E_p (1 + M \cos k_g z) - J/e\mu\langle n \rangle \quad (5.9)$$

Equations 3.17, 5.2, and 5.9 give for this case of $k_g \Lambda \gg 1$,

$$E \cong \gamma_{di} e^{-\gamma_{di} t} E_p M \cos k_g z + E_p M (\cos k_g z) (1 - e^{-\gamma_{di} t})^2 \quad (5.10)$$

As an interesting side point, for an applied field the voltage at small times is E_{app} , and the voltage decays to zero as the space-charge field builds up as time approaches infinity. The space-charge field builds up to cancel the applied-field, given a net zero field. For the photovoltaic case, the electric field is small at small times and approaches E_p as the space-charge field builds up as time approaches infinity. (The field E_p is the space-charge field generated by the photovoltaic effect). The space-charge field builds up and cancels the photovoltaic current, giving a nonzero field.

SECTION 6

DEPLETION AND SATURATION

The conditions for no depletion of the electrons in the N_e levels (which determine the optical absorption coefficient $\beta = \sigma_D N_e$) and no saturation of the available recombination levels N_+ (which determine the effective recombination frequency $\nu_{th} N_+$) are given in Equations 2.17 and 2.18, respectively. The first condition required for no depletion and no saturation is that the steady-state value $(\langle \gamma_{IO} \rangle / \gamma_r) N_{e0}$ of the amplitude of n , from Equations 3.1 and 3.2, must be sufficiently small for Equations 2.17 and 2.18 to be valid. By conservation of electrons, the number of electrons N_{e0} available to be photoexcited at $t = 0$ must always be equal to the total number of electrons

$$N_{e0} = \langle N_e \rangle + \langle n \rangle \quad (6.1)$$

where $\langle \rangle$ is spatial average, as defined in Equation 1.3.

Taking the spatial averages of Equations 2.17 and 2.18 gives

$$|\langle N_{+\Delta} \rangle| \ll N_{+0}, \text{ for negligible saturation} \quad (6.2)$$

and

$$|\langle N_{e\Delta} \rangle| = |\langle N_{+\Delta} \rangle| \ll N_{e0}, \text{ for negligible depletion.} \quad (6.3)$$

From Equation 6.1 and $\langle N_e \rangle - N_{e0} = \langle N_e - N_{e0} \rangle = \langle N_{e\Delta} \rangle$,

$$\langle n \rangle = \langle N_{e\Delta} \rangle. \quad (6.4)$$

Thus, Equations 3.2 and 6.4 give

$$\langle N_{e\Delta} \rangle = (\langle \gamma_I \rangle / \gamma_r) N_{e0} \quad , \quad (6.5)$$

which requires

$$\langle \gamma_I \rangle \ll \gamma_r \quad , \quad \text{for negligible depletion} \quad (6.6)$$

as seen by comparing Equations 6.3 and 6.5.

The corresponding condition for negligible saturation is obtained by writing Equation 6.5 as

$$\langle N_{e\Delta} \rangle = (\langle \gamma_I \rangle / \gamma_r) (N_{e0} / N_{+0}) N_{+0} \quad . \quad (6.7)$$

Comparison of Equations 6.7 and 6.2, with $|N_{+\Delta}| = |N_{e\Delta}|$ from Equation 2.16, gives

$$\langle \gamma_I \rangle \ll (N_{e0} / N_{+0}) \gamma_r \quad , \quad \text{for negligible saturation.} \quad (6.8)$$

The value of $\langle I \rangle$ corresponding to Equation 6.6 is $\langle I \rangle \ll I_{\text{sat}}$, where

$$\begin{aligned} I_{\text{sat}} &= \gamma_r h\nu / \sigma \\ &= 2 \times 10^2 \text{ s}^{-1} (4.0 \times 10^{-19} \text{ J}) / 5 \times 10^{-18} \text{ cm}^2 \\ &= 1.6 \times 10^{11} \text{ W/cm}^2 \quad . \end{aligned} \quad (6.9)$$

This very large typical value of $I_{sat} \cong 10^{11}$ W/cm², compared with typical cw values of 10 W/cm² and rather large pulsed values of 10⁸ W/cm² (1 J/cm² and 10 msec) shows that saturation and depletion are not likely to be problems in fairly heavily doped samples even under short-pulse-duration operation. It is possible that N_{e0}/N_{+0} in Equation 6.8 could be small, thus lowering the saturation threshold. However, in most current high-speed, real-time applications it is desirable to make N_{+0} small and N_{e0} large, so that saturation is negligible (Equation 6.8), if depletion is negligible (Equation 6.6).

In addition to these restrictions (Equations 6.6 and 6.8) on the maximum irradiance I , there are restrictions imposed on the values of N 's in order that the values of $\rho \cong eN_{+\Delta}$ at longer times ($t \gg \tau_r$) can be obtained. For example, the maximum value of E in Equation 3.16 for the case of $J_0 = 0$ and applied field only is, to within a numerical factor of order 1, $E_{app} M$, and the corresponding value of $|N_{+\Delta}|$ from Equation 3.10 with $t = \gamma_{di}^{-1}$ and $\Lambda_{dr} = \mu\tau_r E \cong \mu\tau_r E_{app} M$ is

$$|N_{+\Delta}| = N_{sat} \cong \frac{ck E_{app}^2 M^2}{4\pi e} \quad (6.10)$$

With Equations 6.2 and 6.3, this gives

$$N_{sat} \ll N_{+0}, N_{e0} \quad (6.11)$$

where N_{sat} is defined in Equation 6.10.

According to Equations 6.11 and 6.10, both N_{+0} and N_{e0} must be greater than

$$N_{sat} \cong \frac{6(3 \times 10^5 \text{ cm}^{-1})(10^4 \text{ V/cm})(1/300)(SV/V)}{4\pi \cdot 4 \cdot 10^{-10} \text{ (ergcm)}^{1/2}} = 10^{16} \text{ cm}^{-3} \quad (6.12)$$

for $E_{app} = 10$ kV/cm, $\epsilon = (2.3)^2$, $\sin \theta = 0.5$, $\lambda = 500$ nm, and $M \cong 1$. This is a rather small value of N_{sat} — corresponding to $\sim 10^{16}/5 \times 10^{22} = 2 \times 10^{-7}$ 0.2 part per million of Fe^{2+} and Fe^{3+} . Large dopings are commonly used. Thus, the usual doping are sufficiently large to avoid the long-time saturation and depletion. However, for small values of M , the factor M^2 in Equation 6.10 can make N_{sat} small.

In the general case, N_{sat} must satisfy Equation 6.10, with

$$N_{sat} = \frac{ck}{g} \frac{E_{gmx} M}{4\pi e} , \quad (6.13)$$

where E_{gmx} is the maximum value of the z dependent electric field that gives the grating amplitude.

SECTION 7

STEADY-STATE RESULTS

The steady state has been considered for individual processes in the previous sections. Since the value of $k_g \Lambda$ for all processes affects the individual processes, it is convenient to consider the steady state with all processes included. The key equations for determining the steady state field E are

$$E = (eD\partial n/\partial t + pN_e I - J_0)/e\mu n \quad (7.1a)$$

$$E = (eD\partial n/\partial z + pN_e \langle I \rangle M \cos k_g z + e\mu \langle n \rangle \langle E \rangle)/e\mu n \quad (7.1b)$$

$$E = (eD\partial n/\partial t + pN_e I)/e\mu n, \quad \text{open circuit} \quad (7.1c)$$

$$E = (eD\partial n/\partial z + pN_e \langle I \rangle M \cos k_g z)/e\mu n, \quad \text{short circuit} \quad (7.1d)$$

$$E = (eD\partial n/\partial t + pN_e \langle I \rangle M \cos k_g z + e\mu \langle n \rangle E_{app})/e\mu n, \quad \text{for } \langle E \rangle = E_{app} \quad (7.1e)$$

$$\partial E/\partial z = 4\pi e c^{-1} (N_{+0} - n) \quad (7.2)$$

$$N_{+} = (\gamma_I/\gamma_r) (N_e N_{+0}/n) \quad (7.3)$$

and

$$\langle N_{+\Delta} - r \rangle = 0 \quad (7.4)$$

Equation 7.1 is obtained from the steady-state condition $J = J_0 = \text{constant} \neq f(z, t)$. The average field $\langle E \rangle$ from Equation 7.1a is

$$\langle E \rangle = (pN_e \langle I \rangle - J_0)/e\mu \langle n \rangle \quad (7.5)$$

Solving Equation 7.5 for J_0 and substituting the result into Equation 7.1a gives Equation 7.1b. For an open circuit, setting $J_0 = 0$ in Equation 7.1a gives Equation 7.1c. For a short circuit $\langle E \rangle = 0$, Equation 7.1b reduces to Equation 7.1d. For a voltage $V_{app} = \lambda E_{app}$ applied with ohmic contacts, $\langle E \rangle = E_{app} k$, and Equation 7.1b reduces to Equation 7.1e.

Equation 7.2 is Equation 2.11 with a ρ given by Equation 2.12. Equation 7.3 is obtained from Equation 2.9 with $\partial N_+ / \partial t = 0$.

Equation 7.4 is the quasi charge-neutrality condition, which arises as follows: In general, charge neutrality means that the charge density ρ is zero. Then, integrating Poisson's equation $\nabla \cdot \epsilon E = 4\pi\rho$ gives $E = \text{constant}$ for the current case in which $\epsilon \cong \text{constant}$. (It is easy to show that the spatial dependence of $\epsilon = n_g^2$ corresponding to the spatial dependence of grating index n_g is negligible in the cases considered here). Quasi-charge neutrality in the context of index gratings means that the constant term $\langle \rho \rangle$ in $\rho = \langle \rho \rangle + \rho \Delta$ must equal zero in order to avoid the unphysical term $E \sim \langle \rho \rangle z$ in the electric field. Thus, Equation 2.12 and $\langle \rho \rangle = 0$ give Equation 7.4.

The case of short steady-state electron transport distance is simple. [The condition for this short transport distance will be considered later. Kukhtarev's condition $\xi \ll 1$ and $\xi_g \ll 1$ are sufficient if $\langle n \rangle \ll N_{+0}$, but are not necessary in general. Physically I would expect $k_g \Lambda_{ss} \ll 1$ with $\Lambda_{ss} = \mu E_{ss} \tau_r + (D \tau_r)^{1/2}$.] The electron concentration from Equation 3.1 and 3.2 is $n = \langle n \rangle (1 - M \cos k_g z)$. Substitution into Equation 7.1a gives

$$E_\eta = (E_p \xi M \cos k_g z + E_d M \sin k_g z - J_0 / e \mu \langle n \rangle) / (1 + M \cos k_g z) \quad (7.6)$$

where

$$E_p \equiv \Lambda_p \gamma_r / \mu = p N_e \langle I \rangle / e \mu \langle n \rangle, \quad E_d = D k_g / \mu. \quad (7.7)$$

The term $E_p \xi M \cos k_g z / (1 + M \cos k_g z)$ arises from the deviation of n from $\langle n \rangle (1 + M \cos k_g z)$, as discussed in the derivation of Equation 5.7. [The consistency of E_η in Equation 7.6 with Equations 7.2 to 7.4 will be demonstrated below. This consistency establishes the conditions required for $n = \langle n \rangle (1 + M \cos k_g z)$ to be valid].

The case of long steady-state electron-transport distance requires some care. For example, formally setting $n = \langle n \rangle$ in Equation 7.1 would give

$$E = E_p (1 + M \cos k_g z), \quad \text{for } n = \langle n \rangle. \quad (7.8)$$

This result is incorrect because the deviation in n from $\langle n \rangle$ gives terms in Equation 7.1 that are much greater than E_p in general, as will now be shown. Setting

$$n = \langle n \rangle + n_\delta, \quad N_e = \langle N_e \rangle + N_{e\delta}$$

in Equation 7.3 and using $N_{+\Delta} = N_+ - N_{+0}$ gives

$$N_{+\Delta} - n = \left(\frac{N_{+0}}{1 + n_\delta / \langle n \rangle} \right) \left(\frac{\langle \gamma_r \rangle \langle N_e \rangle}{\gamma_r \langle n \rangle} \right) (1 + M \cos k_g z) (1 + N_{e\delta} / \langle N_e \rangle) - N_{+0} - \langle n \rangle - n_\delta. \quad (7.9)$$

with $n_\delta \ll \langle n \rangle$, which will be verified below, and

$$N_{e\delta} = r \langle N_e \rangle M \cos k_g z. \quad (7.10)$$

and

$$(1 + M \cos k_g z)(1 + r M \cos k_g z) = 1 + \frac{1}{2} r M^2 + (1 + r) M \cos k_g z + \frac{1}{2} r M^2 \cos 2k_g z, \quad (7.11)$$

Equation 7.9 becomes

$$N_{+\Delta} - n = \langle N_{+\Delta} - n \rangle + (N_{+\Delta} - n)_\delta \quad (7.12)$$

where

$$\langle N_{+\Delta} - n \rangle = N_{+0} (g/n - 1 - n) \quad (7.13a)$$

and

$$(N_{+\Delta} - n)_\delta = N_{+0} \frac{\langle \gamma_I \rangle \langle N_e \rangle}{\gamma_r \langle n \rangle} \left[(1 + r) M \cos k_z + \frac{1}{2} r M^2 \cos k_z \right] \quad (7.13b)$$

with

$$g \equiv (\langle \gamma_I \rangle / \gamma_r) (\langle N_e \rangle / N_{+0}) \left(1 + \frac{1}{2} r M^2 \right) \quad (7.14)$$

The factor r in Equation 7.10 is a measure of depletion. For $r \ll 1$, $N_e \cong \langle N_e \rangle \cong N_{e0}$. Since $N_{\Delta e} = -N_{\Delta+}$ from Equation 2.16, assuming that $N_{e\Delta} \cong N_{e\delta}$ and $\langle N_e \rangle \cong N_{e0}$ in Equation 7.10 gives

$$|r| \cong N_{+0} / N_{e0} \quad (7.15)$$

Setting $\langle N_{+\Delta} - n \rangle$ equal to zero, to obtain quasi charge neutrality, gives

$$\eta = (1/4 + g)^{1/2} - 1/2 \quad (7.16a)$$

$$\cong g^{1/2} \quad \text{for } g \gg 1 \quad (7.16b)$$

$$\cong g \quad \text{for } g \ll 1 \quad (7.16c)$$

These results can be written as:

$$\langle n \rangle \cong \left[\langle \gamma_I \rangle \langle N_e \rangle N_{+0} \left(1 + \frac{1}{2} r M^2 \right) / \gamma_r \right]^{1/2} \gg N_{+0} \quad (7.17a)$$

for $\langle \gamma_I \rangle \gg N_{+0} \gamma_r / \langle N_e \rangle$

$$\langle n \rangle \cong (\langle \gamma_I \rangle / \gamma_r) \langle N_e \rangle (1 + \frac{1}{2} r M^2) \ll N_{+0}, \text{ for } \langle \gamma_I \rangle \ll N_{+0} \gamma_r / \langle N_e \rangle \quad (7.17b)$$

We consider only the low-irradiance limit $g \ll 1$. Equation 7.14 and $g \ll 1$ give

$$\langle \gamma_I \rangle \ll N_{+0} \gamma_r / \langle N_e \rangle (1 + \frac{1}{2} r M^2) \quad , \quad (7.18)$$

in which

$$\langle n \rangle = (\langle \gamma_I \rangle / \gamma_r) \langle N_e \rangle (1 + \frac{1}{2} r M^2) \quad , \quad (7.19)$$

which agrees with Equation 3.2 in the limit of negligible depletion, $\langle N_e \rangle \cong N_{e0}$, and $r \ll 1$. Equations 7.14 and 7.19 give

$$(N_{+\Delta} - n)_z \cong N_{+0} \frac{(1+r)M}{1 + \frac{1}{2} r M^2} \cos k_g z + N_{+0} \frac{\frac{1}{2} r M^2}{1 + \frac{1}{2} r M^2} \cos k_g z \quad . \quad (7.20)$$

Substituting Equation 7.20 into Equation 7.2 and integrating gives

$$E = E_q \left[\frac{(1+r)M}{1 + \frac{1}{2} r M^2} \sin k_g z + \frac{rM^2/4}{1 + \frac{1}{2} r M^2} \sin 2k_g z \right] \quad (7.21)$$

where

$$E_q = 4\pi e N_{+0} / \epsilon k_g \quad . \quad (7.22)$$

For negligible depletion the inequality $r \ll 1$ is valid, i.e., $N_{+0} \ll N_{e0}$ from Equation 7.15. With $N_{e\Delta} = -N_{+\Delta}$ from Equation 2.16 and $N_{+\Delta} = N_{+0} M \cos k_g z$ from Equation 7.20 with $n_z \ll N_{+\Delta z}$, the term $N_{e\delta}/\langle E_e \rangle$ in Equation 7.9 is negligible for either $N_{+0} \ll N_{e0}$ or small modulation. In this case of $r \ll 1$, Equation 7.21 gives

$$E = E_q M \sin k_g z, \quad \text{for } g, r \ll 1. \quad (7.23)$$

and Equation 7.14 and $N_+ = N_{+0} + N_{+\Delta}$ give

$$N_+ = N_{+0} (1 + M \cos k_g z), \quad \text{for } g, r \ll 1, \quad (7.24)$$

where $g \ll 1$ is the small-irradiance limit of Equation 7.17b and $r \ll 1$ is the negligible-depletion limit. Thus, for $M \ll 1$ not satisfied, depletion is not negligible ($N_{+\Delta}/N_{+0} = M \cos k_g z$ is not much less than unity).

The result in Equation 7.8 obtained formally (and incorrectly) by using $n = \langle n \rangle$ in Equation 7.1 is negligible with respect to the correct result in Equation 7.23, i.e.,

$$E_p/E_q = k_g \Lambda \epsilon \gamma_r / 4\pi e \mu N_{+0} = 3.7 \times 10^{-5} \ll 1. \quad (7.25)$$

From Equation 5.5, we have $\xi_T = E_d/E_q$. Thus, $E_q \ll E_d$ for $\xi_T \gg 1$. With Equation 7.25 this gives

$$E_p \ll E_q \ll E_d \quad \text{for long transport distance.} \quad (7.26)$$

The following check on the consistency of Equations 7.23 and 7.1 is not essential to the understanding of the control results. The small deviations in n from the large term $\langle n \rangle$ are retained and shown to be small and to account for the result in Equation 7.23. The field E in Equation 7.23 comes from the first term

in Equation 7.1. The small deviation in n from $\langle n \rangle$ must be retained in Equation 7.1 in order to obtain Equation 7.23. First consider the short-circuit case of Equation 7.1c. The second term in Equation 7.1c is negligible as shown in Equation 7.26. Setting $n = \langle n \rangle (1 + n_c M \cos k_g z)$ in Equation 7.1c and equating the resulting E to the E in Equation 7.23 gives, with $Dk_g/\mu = E_d$,

$$E_d n_c M \sin k_g z = E_q M \sin k_g z .$$

Solving for n_c gives

$$n_c = E_q/E_d = 4\pi e N_{+0} \mu / \epsilon D k_g^2 \cong 1/\epsilon_T \ll 1 \quad (7.27)$$

where ϵ_T is Debye-length parameter of Kukhtarev and coworkers.

For the open-circuit case of Equation 7.1c defining $n = \langle n \rangle (1 + n_{cs})$, where $n_{cs} = n_c M \cos k_g z + n_s M \sin k_g z$, and using $(1 + n_{cs})^{-1} \cong 1 - n_{cs}$ for $n_{sc} \ll 1$ and setting the resulting E equal to the E in Equation 7.23 gives

$$E_d n_c M \sin k_g z - E_d n_s M \cos k_g z + E_p M \cos k_g z - E_p n_c M \cos k_g z - E_p n_s M \sin k_g z = E_q M \sin k_g z .$$

Setting the sum of the coefficients of the $\cos k_z$ terms equal to zero gives

$$n_s = E_p/E_d = \Lambda_p k_g / \Lambda_d^2 k_g^2 \ll 1 \quad (7.28)$$

where $\Lambda_p k_g \ll 1$ is always satisfied and $\Lambda_d^2 k_g^2 \gg 1$ is satisfied in the long transport limit. Setting the sum of the coefficients of the $\sin k_g z$ terms equal to zero gives

$$n_c = \frac{E_q + E_p n_s}{E_d} \ll 1$$

where $E_q/E_d \ll 1$ from Equation 7.27, $n_s \ll 1$ from Equation 7.28, and $E_p/E_d \ll 1$ from Equation 7.28.

SECTION 8

RESULTS OF KUKHTAREV AND COWORKERS AND OF AMODEI

Several results of Kukhtarev and coworkers³ and of Amodei² are discussed in order to show the relation between the present results and the results of these previous important papers and moreover to resolve inconsistencies among the three sets of results.

Kukhtarev and coworkers consider only the steady state. We set their thermal generation factor β equal to zero because the levels of interest here are too deep for thermal generation of free carriers to be important. We also neglect the small correction to M for the case of $k_g \Lambda \ll 1$ even though it should be simple to obtain this correction from the present model. The relations between Kukhtarev's notation and ours are as follows:

$$\begin{array}{lll}
 f \rightarrow \gamma_I & N_D^+ \rightarrow N_+ & N_A \rightarrow N_{+0} \\
 \gamma_R \rightarrow \gamma_r / N_{+0} & \cos(2k_x x + \phi) \rightarrow \cos k_g z & \mu T / |e| \rightarrow D \\
 T \rightarrow k_B T & \xi_T \rightarrow E_d / E_q & \xi_E \rightarrow (E_{app} + E_p) / E_q
 \end{array}$$

Their condition

$$\gamma_I \ll \gamma_r n / N_{+0} \quad (8.1)$$

is valid only in samples having many more filled levels than empty levels, that is,

$$N_{+0} \ll N_{e0} \quad (8.2)$$

This can be seen as follows. Setting $\partial N_+ / \partial t = 0$ and $N_e = N_p + N_{+0}$ in Equation 2.9 and solving for N_+ gives

$$N_+ = \frac{\gamma_I N_D}{\gamma_I + \gamma_r n / N_{+0}} \quad (8.3a)$$

$$\cong (\gamma_I / \gamma_r) N_D N_{+0} / n \quad (8.3b)$$

where the approximate equality in Equation 8.2b is valid when the Kukhtarev- and coworkers inequality in equation 8.1 is valid. Again setting $\partial N_+ / \partial t = 0$ in Equation 2.9, but retaining N_e , and using Equations 2.14 to 2.16 gives

$$n = \left(n_{\text{unsat}} \right) \left(\frac{1 - N_{+\Delta} / N_{e0}}{1 + N_{+\Delta} / N_{+0}} \right), \quad (8.4)$$

where

$$n_{\text{unsat}} = (\gamma_I / \gamma_r) N_{e0} = \langle \gamma_I \rangle / \gamma_r N_{e0} (1 + M \cos k_g z) \quad (8.5)$$

Equation 8.3b can be rewritten as

$$n = n_{\text{unsat}} (N_D / N_{e0}) \frac{1}{1 + N_{+\Delta} / N_{+0}} \quad (8.6)$$

The exact result in Equation 8.4 reduces to the approximate result in Equation 8.6 if $N_D \cong N_{e0}$. Then $N_{+0} \ll N_{e0}$, the factor $N_{+\Delta} / N_{e0}$ is negligible in the negligible-saturation limit, and the factor $N_D / N_{e0} \cong 1$ in Equation 8.5.

Equation 9 of Kukhtarev and coworkers with $m = M$ is in agreement with Equations 3.12, 4.8, and 5.3. Thus, our results and theirs agree for the short-transport distance limit of $k_g \Lambda \ll 1$. Their Equation 9 is valid even when their approximation $N_{+0} \ll N_D$ is not satisfied.

Next consider the limit $k_g \Lambda \gg 1$. From Equation 8.6 with the Kukhtarev and coworkers approximation $N_D/N_{e0} \cong 1$, in order to have $n \cong \langle n \rangle$ we must have

$$N_{+\Delta} = N_{+0} M \cos k_g z \quad (8.7)$$

so that the factor $(1 + N_{+\Delta}/N_{+0})^{-1}$ in Equation 8.6 cancels the factor $(1 + M \cos k_g z)$ in n_{unsat} (see Equation 8.5). Notice that in this case of $N_{+0} \ll N_D$, the steady state is not reached until N_{+0} is "fully saturated" for $M \cong 1$, that is,

$$N_+ = N_{+0} (1 + M \cos k_g z) . \quad (8.8)$$

The charge density from Equation 2.5 is

$$\rho = e(N_{+\Delta} - n). \quad (8.9)$$

With $n \ll N_{+\Delta}$, substituting Equations 8.9 and 8.8 into Equation 2.11 and integrating gives

$$E = \langle E \rangle - E_q M \sin k_g z \quad (8.10)$$

where $\langle E \rangle$ is the obvious constant of integration and

$$E_q = 4\pi e N_{+0} / \epsilon k_g , \quad (8.11)$$

is in agreement with Equation 7 of Kukhtarev and coworkers.

Finally, notice that Equation 8.10, which is Equation 7 of Kukhtarev and coworkers, is incorrect for the case of an applied field only and an open circuit because Equation 2.10 with $J = D = p = 0$ gives $E = 0$ for $n \neq 0$. The diffusion term in Equation 2.10 and the small deviation n_D in n from $\langle n \rangle$ are needed to establish the field in Equation 8.10 even though D does not appear in the result (because the $1/D$ in n_D cancels the explicit factor D in Equation 8.13).

Amodei² obtained the diffusion-dominated result

$$E \cong \frac{E_d M \sin k_g z}{1 + M \cos k_g z}, \quad (8.12)$$

even in the limit of $\Lambda_{diff} k_g \gg 1$. This result disagrees with the present result in Equations 7.21 or 7.23 and with the result in Equation 8.10 from Kukhtarev and coworkers. The reason for the disagreement is that Amodei assumes that N_{e0} (his N) and N_{+0} (in his $\tau = 1/\gamma_r$) are constant. Then

$$n = \langle n \rangle (1 + M \cos k_g z) \quad (8.13)$$

rather than $n = \langle n \rangle$, as obtained here by Kukhtarev and coworkers

This result in Equation 8.12 is not correct in general because the changes in the values of N_+ and N_e cannot be neglected in the steady state in general. For example, N_{+0} was fully saturated in the case above, according to Equation 8.8. Equation 8.13 is physically implausible for this case of $k_g \Lambda \gg 1$ because the transport distance is greater than the distance k_g over which $\langle I \rangle M \cos k_g z$ changes substantially and the electrons cannot remain in the region in which they are generated if they diffuse or drift such a long distance before recombining.

The result in Equation 8.12 is also inconsistent with the value of E obtained from Poissons equations. For $N_{+0} = \text{constant}$, $N_{+0} = 0$, and Equation 2.5 gives

$$\rho = -en = -e\langle n \rangle (1 + M \cos k_g z) . \quad (8.14)$$

Substituting the z -dependence term into Equation 2.11 and integrating gives

$$E = -(4\pi e\langle n \rangle M / \epsilon k_g) \sin k_g z ,$$

which does not agree with Equation 8.12. Finally, the constant term in ρ in Equation 8.14 does not vanish, as required by quasi-charge neutrality.

SECTION 9
PHOTOVOLTAIC EFFECT

In photovoltaic materials, a space-charge field is believed to be generated by asymmetric photoemission of conduction electrons.¹ In such ferroelectric materials as LiNbO_3 and BaTiO_3 , ions can have potentials that are asymmetric along some direction. For example, the titanium ion in BaTiO_3 is displaced from the center of the lattice cell in the ferro-electric state. Thus, the photogenerated electrons are emitted preferentially in one direction, which gives rise to the photovoltaic field E_p as follows: By definition of the momentum transport time τ_k , the initial momentum is lost in time τ_k on the average. The displacement of the photogenerated electrons during the time τ_k has a typical value $\ell_p = v\tau_k = (10^7 \text{ cm/s})(10^{-14} \text{ s}) = 1 \text{ nm} (= 10 \text{ \AA})$. All of the electrons are not photoemitted along the same direction, but there is a greater probability of emission along the photovoltaic direction. Thus, an effective distance Λ_p is defined as

$$\Lambda_p = p_+ \ell_{p+} - p_- \ell_{p-} \equiv (p_+ - p_-) \ell_p \equiv p_+ \ell_p \quad (9.1)$$

where p_+ and p_- are the probabilities of emission in the + and - directions, respectively.

A typical value of

$$\Lambda_p = 0.08 \text{ nm} (= 0.8 \text{ \AA}) \quad (9.2)$$

is consistent with typical observed photovoltages, as shown below. Equations 3.1 and 9.2 give $P_+ = \Lambda_p / \ell_p = 0.08 \text{ nm} / 1 \text{ nm} = 0.08$ as the relative probability for emission in the positive photovoltaic direction. The short distance of 0.08 nm, which is less than an atomic spacing, is not the actual transport distance, which would be unrealistically short. Rather, it is the weighted distance, as in Equation 9.1.

In the literature,³ it is common practice to model the photovoltaic effect by including the term

$$J_p = p_k I \hat{c} \quad (9.3)$$

in the current, where p_k is a constant and \hat{c} is a unit vector in the opposite direction from the preferred electron emission direction. The following derivation shows that Equation 9.3 is consistent with Glass' preferential emission model if the constant p_k is replaced by $p N_{de}$, where p is a constant and N_{de} is the trapped electron density:

$$J_p = p N_e I \hat{c} \quad (9.4)$$

Equation 9.4, but not Equation 9.3, is equivalent to Glass' expression $J = \kappa \alpha I$ because the absorption coefficient α is proportion to N_e . Equations 9.3 and 9.4 are equivalent in the limit of no depletion ($N_e = N_{e0} = \text{constant}$).

Equation 9.4 is obtained by considering the generation rate of electron by the field

$$(\partial n / \partial t)_I = (\sigma_D / \hbar \omega) I (z - \Lambda_p) N_e (z - \Lambda_p) \quad (9.5)$$

The electrons generated from optical-donor levels at $z - \Lambda_p$ appear at the displaced position z . To Taylor expand in N_e gives

$$(\partial n / \partial t)_I = \sigma_D I(z) N_e(z) / \hbar \omega - \partial (\Lambda_p \sigma_D I(z) N_e(z) / \hbar \omega) / \partial z \quad ,$$

which is of the usual form

$$\partial n / \partial t = \sigma_D I N_e / \hbar \omega - e^{-1} \partial J / \partial z$$

if we set

$$\tilde{J} = J_p = pN_e \hat{C} \quad , \quad (9.6)$$

where $\hat{C} = -\hat{z}$ and

$$p = e\Lambda_p \sigma_D / h\omega \quad . \quad (9.7)$$

We shall use J_p in Equation 9.6, rather than the previous expression in Equation 9.3.

The photovoltaic field that develops in the steady state under open-circuit conditions (that is, $J = \langle n \rangle e\mu E + pN_e \langle I \rangle = 0$) is:

$$E_p = pN_e \langle I \rangle / \langle n \rangle e\mu = \Lambda_p \gamma_r / \mu \quad . \quad (9.8)$$

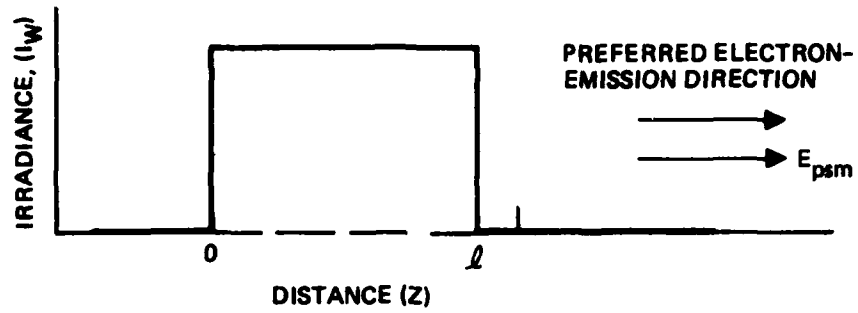
The time constant for E_p to approach the steady state value in Equation 9.8 is the dielectric relaxation frequency γ_{di} , defined in Equation 3.7, as usual.

A small photovoltage

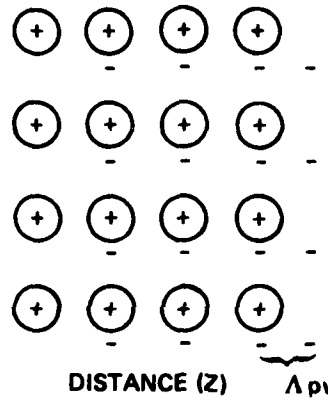
$$E_{psm} = 4\pi E \langle n \rangle \Lambda_p / \epsilon = (\gamma_{di} / \gamma_r) E_p \quad (9.9)$$

is developed in the short-time τ_r , as seen in the following model. Figure 4 schematically illustrates the charge distributions resulting from the displacement of the electrons, denoted by $-$, in the positive z direction by a distance Λ_p . The resulting net charge density in Figure 4 is approximated by δ -functions.

$$\rho = e \langle n \rangle \Lambda_p [\delta(z) - \delta(z - \Lambda_p)]$$



(a) IRRADIANCE DISTRIBUTION



(b) RESULTING CHARGE ARRANGEMENT

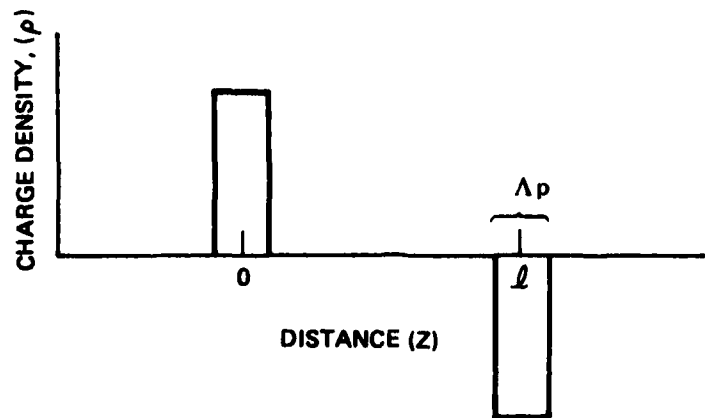
(c) RESULTING CHARGE DENSITY, ρ

Figure 4. Model for the photoelectric effort showing the idealized charge distribution resulting from net electron emission in the positive z direction.

where the electron concentration $\langle n \rangle$ develops in a characteristic time τ_r . Integrating Poisson's equation, $\epsilon dE/dz = 4\pi\rho$ gives,

$$\begin{aligned} E &= E_{psm} && \text{for } 0 < z < \ell \\ &= 0 && \text{for all other values of } z \end{aligned}$$

where E_{psm} is given by Equation 9.9. Since E_p develops in time τ_{di} and E_{psm} develops in time τ_r , it is reasonable that $E_{psm} = (\tau_r/\tau_{di})E_p = (\gamma_{di}/\gamma_r)E$, as in Equation 9.9.

SECTION 10

MODEL OF DIELECTRIC RELAXATION

The following model illustrates the significance of the dielectric relaxation frequency:

$$\gamma_r \equiv 1/\tau_r = 4\pi\sigma/\epsilon = 4\pi e\langle n \rangle/\epsilon \quad , \quad (10.1)$$

which is the time required to change or discharge a sample. Consider a dielectric sample in an externally applied electric field E_{app} , with open circuit conditions, as illustrated in Figure 5. At time $t = 0$, the sample is uncharged. The electric field E_{app} causes a current

$$J_0 = e\mu\langle n \rangle E_{app}$$

at time $t = 0$. The divergence of the current at the end-faces of the sample causes the end-faces to charge up, according to the continuity equation

$$\partial\rho/\partial t = -\partial J/\partial z \quad (10.2)$$

where ρ is the charge density. For

$$J(z,t) = -e\mu\langle n \rangle E(t)r(z) \quad (10.3)$$

where

$$\begin{aligned} r(z) &= 1 && \text{for } 0 < z < \ell \\ &= 0 && \text{for all other values of } z \quad , \end{aligned} \quad (10.4)$$

Equation 10.2 gives

$$\partial\rho/\partial t = -e\mu\langle n \rangle E(t)\Lambda(z) \quad , \quad (10.5)$$

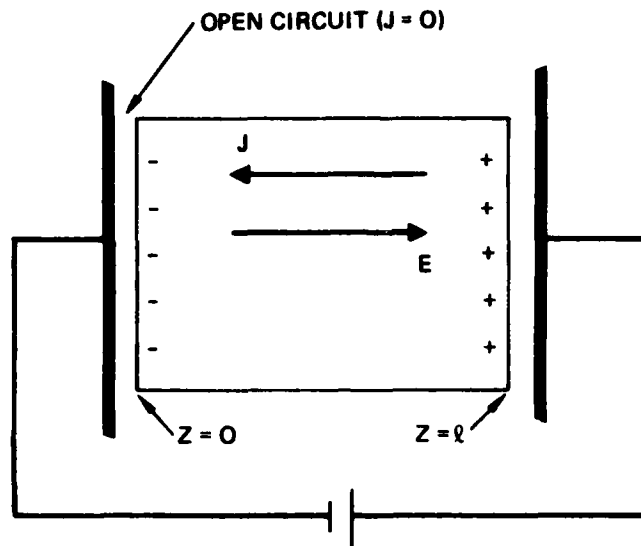


Figure 5. Crystal with an applied field with open-circuit conditions at the faces of the crystal showing the current density J , electric field E , and charged faces of the crystal.

where

$$\Delta(z) = \delta(z) - \delta(z - \ell) . \quad (10.6)$$

Here $\delta(z)$ is the Dirac δ -function, and $dr(z)/dz = \Delta(z)$.

From Poisson's equation,

$$\begin{aligned} \rho &= \epsilon(4\pi)^{-1} \partial E / \partial z = \epsilon(d4\pi)^{-1} \partial [E(t)r(z)] / \partial z \\ &= \epsilon d(4\pi)^{-1} E(t) \Delta(z) . \end{aligned} \quad (10.7)$$

Taking the time derivative of ρ with respect to time in Equation 10.7 and substituting the result into Equation 10.5 gives

$$\partial E(t) / \partial t = -(4\pi \epsilon \mu \langle n \rangle / \epsilon) E(t) . \quad (10.8)$$

For $E(t) = E_{app}$ at $t = 0$, the solution to Equation 10.8 is

$$E(t) = E_{app} e^{-\gamma_{di} t} , \quad (10.9)$$

where γ_{di} is the dielectric relaxation frequency defined in Equation 10.1.

The model illustrates that the time constant for the development of the final charge density ($\rho = \rho_0 \Delta(z)$), which corresponds to the charged end faces of the sample) is the dielectric-relaxation time. The electric field and current decay to zero as the end faces of the sample charge up.

Using the same model, but with $E_{app} = 0$ and $\rho = \rho_0 \Delta(z)$ at time $t = 0$, it is easy to show that an initial charge decays with time-constant $1/\gamma_{di}$:

$$E = E_0 e^{-\gamma_{di} t} . \quad (10.10)$$

The current and electric field decay to zero as the end-face charge decays to zero.

SECTION 11

SUMMARY OF RESULTS

A list of symbols and typical values of parameters is given in the Appendix. Key results for the grating electric field E_g , which is the z-dependent part of $E = E_{app} + E_{sc}$ (which excludes the electric field of the laser irradiance), are listed below.

The corresponding value of the grating index is given by Equation 1.1 and repeated here

$$n_g = \frac{1}{2} n_r^3 rE \quad , \quad (1.1)$$

and the corresponding grating efficiency is given by an expression such as Equation 1.5 and repeated here, i.e.,

$$\eta = e^{-\alpha d / \cos \theta} \sin^2 \frac{\pi n_r n_g d}{2\lambda \cos \theta} \quad . \quad (1.5)$$

The notation for the various cases of E below is as follows:

E_{app} : applied field dominated

D: diffusion dominated

p: photovoltaic-effect dominated

t: short-time solution (τ_r t τ_{di})

ss: steady-state

Λ_{ing} : $k_g \Lambda \gg 1$

Λ_{sht} : $k_g \Lambda \ll 1$

ngbl: negligible depletion and saturation.

Combining the results of Sections 3 through 7 gives the following key results:

From Equations 3.18, 4.9, 5.7 and 7.7, for $k_g \Lambda \ll 1$

$$E \cong \gamma_{di} t e^{-\gamma_{di} t} \left[(E_{app} + E_p) M \cos k_g z + \frac{1}{2} E_d M \sin k_g z \right]$$

$$\times \left(\frac{E_p \xi M \cos k_g z - J_0 / e\mu \langle n \rangle + E_d M \sin k_g z}{1 + M \cos k_g z} \right) \quad (11.1)$$

$$\times \left(1 - e^{-\gamma_{di} t} \right)^2, \text{ for } \Lambda_{short} \text{ negligible}$$

where

$$J_0 / e\mu \langle n \rangle = 0 \quad \text{for open circuit} \quad (11.2a)$$

$$= E_p \quad \text{for short circuit} \quad (11.2b)$$

$$= E_p - E_{app} \quad \text{for } E_{app} \text{ with ohmic contents} \quad (11.2c)$$

From Equations 3.28, 4.11, 5.9, and 7.20, for $k_g \Lambda \gg 1$,

$$E = \gamma_{di} t e^{-\gamma_{di} t} (E_\Lambda + E_p) M \sin k_g z$$

$$+ E_q \left[\frac{(1+r) M}{1 + \frac{1}{2} r M^2} \sin k_g z + \frac{r M^2 / 4}{1 + \frac{1}{2} r M^2} \sin 2k_g z \right] \quad (11.3)$$

$$\times \left(1 - e^{-\gamma_{di} t} \right)^2 .$$

AD-A123 233

PHASE CONJUGATE OPTICS(U) HUGHES RESEARCH LABS MALIBU
CA G J DUNNING ET AL. NOV 82 RADC-TR-82-288
F19628-80-C-0185

2/2

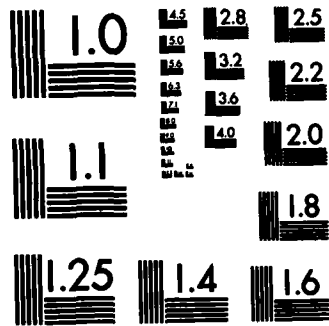
UNCLASSIFIED

F/G 20/6

NL



END
FORMED
BY
DATE



MICROCOPY RESOLUTION TEST CHART
NATIONAL BUREAU OF STANDARDS-1963-A

The results for the phase shifts between the grating electric field and the grating irradiance $\langle I \rangle M \cos k_g z$ are summarized for the various combination of long- and short- electron-diffusion distances and drift (in applied or photovoltaic field) and diffusion-limited transport in Table 2.

Table 2. Spatial Phase Shift Between the Grating (i.e., Photofractive Electric Field E) and Irradiance I.

	$k_g \Lambda \ll 1$		$k_g \Lambda \gg 1$	
	Drift	Diffusion	Drift	Diffusion
Phase	π	$-\pi/2$	$\pi/2$	$\pi/2$

REFERENCES

1. A.M. Glass, "The Photorefractive Effect," *Optical Engineering*, 17, 470-479 (1978).
2. Juan J. Amodei, "Analysis of Transport Processes During Holographic Recording in Insulators," *RCA Review*, 32, 185-198 (1971).
3. N.V. Kukhtarev, V.B. Markov, S.G. Odulov, M.S. Soskin and V.L. Vinetskii, "Holographic Storage in Electro-optic Crystals," *Ferroelectrics*, 22, 949-960, (1979).
4. Albert Rose, Concepts in Photoconductivity and Allied Problems, Interscience Tracts on Physics and Astronomy (Interscience Publishers, New York, 1963).

APPENDIX B

LIST OF SYMBOLS, EQUATIONS, TYPICAL VALUES OF PARAMETERS, UNITS, AND CONVERSION FACTORS

The values of parameters listed below are only estimates. They are for lithium niobate. Values of most of the parameters are unknown. The concentrations c_e and c_+ of full- and empty-optical-donor levels are explicitly displayed in the equation. Two typical values of interest are $c = 0.2$ percent Fe = 2×10^3 ppm of Fe for very heavily doped lithium niobate and $c = 100$ ppm for moderate doping.

c_e (ppm) = concentration of N_e in atomic parts per million

c_+ (ppm) = concentration of N_+ in atomic parts per million

c_e or c_+ = 100 ppm, for Case I

= 2×10^3 ppm = 0.2 percent, for Case II

D = electron diffusion coefficient

= $\mu k_B T / e$

= 0.46 cm²/sec

E_d = diffusion electric field

$$= Dk_g/\mu = k_B T k_g/e$$

$$= 24.2 \text{ statvolts/cm} = 7.75 \text{ kV/cm}$$

E_p = photovoltaic electric field

$$= \Lambda_p \gamma_r/\mu$$

$$= c_+(ppm) 2.26 \text{ V/cm} = c_+(ppm) 7.6 \times 10^{-3} \text{ statvolts/cm}$$

E_q = characteristic steady-state, long-transport-distance electric field

$$= 4\pi e N_{+0}/\epsilon k_B$$

$$= c_+(ppm) 204 \text{ statvolts/cm} = c_+(ppm) 61 \text{ kV/cm}$$

E_Λ = characteristic electron-drift electric field

$$= \gamma_r/\mu k_g$$

$$= c_+(ppm) 1.0 \text{ kV/cm}$$

$\hbar\omega$ = photon energy

$$= 4.0 \times 10^{-19} \text{ J} = 4.0 \times 10^{-12} \text{ erg} = 2.5 \text{ eV, for } \lambda = 500 \text{ nm}$$

I = assumed sinusoidal irradiance distribution for writing a grating

$$= \langle I \rangle (1 + M \cos k_g z)$$

$\langle I \rangle$ = spatial average of I

$$= 130 \text{ W/cm}^2 = 1.3 \times 10^9 \text{ erg/scm, for 10 mW at diameter } d = 0.1 \text{ mm}$$

J_p = photovoltaic current

$$= p N_e I$$

$$= c_e (\text{ppm}) 62.4 \text{ statamps/cm}^2 = c_e (\text{ppm}) 2.1 \times 10^{-8} \text{ A/cm}^2$$

k_g = grating wavevector

$$= 4\pi n_r (\sin \theta) / \lambda$$

$$= 2.8 \times 10^5 \text{ cm}^{-1} = (3.6 \times 10^{-6} \text{ cm})^{-1}$$

M = modulation factor in the irradiance

N_e = concentration of Fe^{2+} , filled optical-donor levels

N_{e0} = value of N_e at $I = 0$.

$$= c(\text{ppm}) \times 5 \times 10^{16} \text{ cm}^{-3}$$

$$= 5 \times 10^{18} \text{ cm}^{-3} \quad \text{for } c = 100 \text{ ppm}$$

$$= 10^{20} \text{ cm}^{-3} \quad \text{for } c = 0.2 \text{ percent} = 2 \times 10^3 \text{ ppm}$$

$$N_{e\Delta} \equiv N_e - N_{e0}$$

N_+ = concentration of Fe^{3+} , empty optical-donor levels, that is, recombination levels

N_{+0} = value of N_+ at $I = 0$

$$= c(\text{ppm}) \times 5 \times 10^{16} \text{ cm}^{-3}$$

$$N_{+\Delta} \equiv N_+ - N_{+0}$$

$\langle n \rangle$ = spatial average of the conduction-electron density

$$= (\langle \gamma_I \rangle / \gamma_r) N_{e0} = \sigma_D \langle I \rangle N_{e0} / h\nu \gamma_r$$

$$= \left[c_e(\text{ppm}) / c_+(\text{ppm}) \right] (I / 130 \text{ Wcm}^{-2}) 3.2 \times 10^9 \text{ cm}^{-3}$$

n_g = grating index

$$= 1/2 n^3 rE$$

$$= 6.1 \times 10^{-4} \quad \text{for } E = 10 \text{ kV}$$

n_r = real part of the refractive index

$$= 2.3$$

p = photovoltaic coupling constant (in the expression $J_p = pN_e I$)

$$= e\lambda_p \sigma_D / \hbar\omega$$

$$= 9.6 \times 10^{-25} \text{ cm}^{7/6} / \text{erg}^{1/2}$$

r = appropriate linear electro-optic coefficient (in Equation 1.1)

$$= 10^{-8} \text{ cm/V} \quad \text{from Glass}^1$$

s = cross section for recombination, which is the capture of electron by an empty optical-donor level

$$= 10^{-14} \text{ cm}^2, \text{ reasonable value for a deep, charged impurity}$$

t = time of laser irradiation or time to erase

v_{th} = thermal velocity of conduction electrons

$$= 10^7 \text{ cm/s} \quad \text{at room temperature}$$

GREEK SYMBOLS:

α = optical absorption coefficient

$$= 40 \text{ cm}^{-1} \quad \text{for 0.2 percent Fe in the melt (assumed to give 0.1 percent Fe in the crystal)}^1$$

ϵ = dielectric constant

$$= (2.3)^2 = 5.29$$

γ_{di} = dielectric relaxation frequency

$$= 4\pi\epsilon\mu <n>/\epsilon$$

$$= 4\pi\epsilon\mu \sigma_D <I> N_{e0}/\epsilon h\omega_{th} s N_{+0}$$

$$= \left[c_e(\text{ppm})/c_+(\text{ppm}) \right] (I/130 \text{ Wcm}^{-2}) 1.93 \times 10^4 \text{ s}^{-1}$$

$$= \left[c_e(\text{ppm})/c_+(\text{ppm}) \right] (I/130 \text{ Wcm}^{-2}) (5.17 \times 10^{-2} \text{ ms})^{-1}$$

$<\gamma_I>$ = spatial average of the optical-pumping frequency γ_I

$$= \sigma_D <I>/h\omega$$

$$= 325 \text{ s}^{-1} = 1/3.1 \text{ msec}$$

$\gamma_r = 1/\tau_r$ = recombination of electrons and empty optical-donor levels for the case of negligible saturation, $N_+ = N_{+0}$

$$= v_{th} s N_{+0}$$

$$= c_+(\text{ppm}) 5 \times 10^9 \text{ sec}^{-1} = c_+(\text{ppm})/0.2 \text{ nsec}$$

Λ_d = electron-diffusion transport distance

$$= (D/\gamma_T)^{1/2}$$

$$= c_+(\text{ppm})^{-1/2} 9.6 \times 10^{-6} \text{ cm}$$

Λ_E = electron-drift transport distance

$$= \mu E/\gamma_T$$

$$= c_+(\text{ppm})^{-1} 3.5 \times 10^{-5} \text{ cm} \quad \text{for } E = 10 \text{ kV/cm}$$

Λ_p = photovoltaic characteristic diffusion length

$$= 8 \times 10^{-9} \text{ cm}, \quad \text{from Glass}^1$$

λ = wavelength of the laser radiation

$$= 500 \text{ nm}$$

μ = electron mobility

$$= 5.3 \times 10^3 \text{ cm}^2/\text{s statvolt} = 17.6 \text{ cm}^2/\text{Vs}$$

ω = laser frequency

$$= (500 \text{ nm}/\lambda) 3.77 \times 10^{15} \text{ sec}^{-1}$$

ρ = charge density

σ_D = optical cross section for optical excitation of an electron
into the conduction band

$$= 10^{-18} \text{ cm}^{-1}, \text{ estimated from Glass}^1 \text{ values of } \alpha = 40 \text{ cm}^{-1} \\ \text{for } N_{e0} = 0.5 (2 \times 10^{-3}) 5 \times 10^{22} \text{ cm}^{-3}; \sigma_D = \alpha/N_{e0} = \\ 8 \times 10^{-19} \text{ cm}^{-1}$$

θ = half angle in the material between the direction of
propagation of the two beams that write the grating.

ζ_E = Kukhtarev-and-coworker³ transport parameter

$$= (E_{app} + E_p)/E_q$$

$$= 0.16/c_+ (\text{ppm})$$

ζ_T = Kukhtarev-and-coworker transport parameter

$$= E_d/E_q$$

$$= 0.12/c_+ (\text{ppm})$$

The following electrostatic units (esu) and conversions are listed for the convenience of the reader. Brackets denote "the units of."

$$[e] = (\text{erg cm})^{1/2}$$

$$[e\mu] = \text{cm}^3/\text{sec}$$

$$[E] = (\text{erg/cm}^3)^{1/2}$$

$$[\mu] = \text{cm}^{5/2}/\text{erg}^{1/2} \text{ sec}$$

$$[\text{statvolts}] = (\text{erg/cm})^{1/2}$$

$$1 \text{ erg} = 10^{-7} \text{ J}$$

$$1 \text{ statamp} = 3.34 \times 10^{-10} \text{ A}$$

$$1 \text{ statvolt} = 300 \text{ V}$$

APPENDIX C

BIBLIOGRAPHY — PHOTOREFRACTIVE EFFECT

- J.J. Amodei, *Appl. Phys. Lett* 18, 22 (1971). SrTiO₃
- J.J. Amodei, D.L. Staebler, and A.W. Stephens, *Appl. Phys. Lett.* 18, 507 (1971). Ba₂NaNb₅O₁₅
- J.J. Amodei, *RCA Review* 32, 185 (1971) LiNbO₃
- A. Ashkin, G.D. Boyd, J.M. Dziedzic, R.G. Smith, A.A. Ballman, J.J. Levinstein, and K. Nassau, *Appl. Phys. Lett* 9, 72 (1966) LiNbO₃, LiTaO₃
- F.S. Chen, *J. Appl. Phys.* 38, 3418 (1967). LiNbO₃
- F.S. Chen, *Appl. Phys. Lett* 13, 223 (1968). LiNbO₃
- F.S. Chen, *J. Appl. Phys.* 40, 3389 (1969). LiNbO₃, LiTaO₃
- Che-Tsung Chen, Dae M. Kim, and D. Von Der Linde, *IEEE J. Quantum Electron* QE-16, 12 (1980). LiNbO₃
- B.W. Faughnan and Z.J. Kiss, *Phys. Rev. Lett* 21, 1331 (1968). SrTiO₃, TiO₂
- J. Feinberg and R.W. Hellwarth, *Opt. Lett* 5, 519 (1980). BaTiO₃
- J. Feinberg, D. Heiman, A.R. Tanguay, and R.W. Hellwarth, *J. Appl. Phys.* 51, 1297 (1980). BaTiO₃
- B. Fischer, M. Cronin-Golomb, J.O. White, and A. Yariv, *Optics Lett.*, To be published (1981). Analysis
- A.M. Glass, D. Von Der Linde, D.H. Auston, and T.J. Negran, *J. Electron. Materials* 4, 915 (1975). Review
- A.M. Glass, *Opt. Engin.* 17, 470 (1978). Review
- P. Gunter, U. Fluckiger, J.P. Huignard, and F. Micheron, *Ferroelectrics* 13, 297 (1976). KNbO₃
- P. Gunter and F. Micheron, *Ferroelectrics* 18, 27 (1978). KNbO₃
- P. Gunter, *Ferroelectrics* 22, 671 (1978). KNbO₃
- P. Gunter and A. Krumins, *Appl. Phys.* 23, 199 (1980). KNbO₃
- P. Gunter, *Optics Lett.*, To be published (1981). KNbO₃, BGO
- J.P. Hermann, J.P. Herriau and J.P. Huignard, *Appl. Opt.* 20, 2173, (1981). BSO

J. Herriau, J. Huignard, and P. Aubourg, Appl. Opt. <u>17</u> , (1978).	BSO
J.P. Huignard and F. Micheron, Apl. Phys. Lett. <u>29</u> , 591 (1976).	BSO, BGO
J.P. Huignard, J.P. Herriau, P. Aubourg, and E. Spitz, Opt. Lett. <u>4</u> , 21 (1979).	BSO
J.P. Huignard, J.P. Herriau, G. Rivet, and P. Gunter, Opt. Lett. <u>5</u> , 102 (1980).	BSO
W.D. Johnston, Jr., J. Appl. Phys. <u>41</u> , 3279 (1970).	LiNbO ₃
D.M. Kim, Rajiv R. Shah, T.A. Rabson, and F.K. Tittel, Appl. Phys. Lett. <u>28</u> , 338 (1976).	Analysis
E. Kratzig and R. Orlowski, Appl. Phys. <u>15</u> , 133 (1978).	LiTaO ₃
E. Kratzig and R. Orlowski, Opt. and Quant. Electron. <u>12</u> , 495 (1980).	LiNbO ₃ , LiTaO ₃
E. Kratzig, F. Welz, R. Orlowski, V. Doormann, and M. Rosenkranz, Solid St. Comm. <u>34</u> , 817 (1980).	BaTiO ₃
A. Krumins and P. Gunter, Appl. Phys. <u>19</u> , 153 (1979).	KNbO ₃
A.E. Krumins and P. Gunter, Phys. Stat. Sol. <u>A55</u> , K185 (1979)	KNbO ₃
A. Krumins and P. Gunter, Phys. Stat. Sol. <u>A63</u> , K111 (1981).	KNbO ₃
N. Kukhtarev, V. Markov, and S. Odulov, Opt. Comm. <u>23</u> , 338 (1977).	LiNbO ₃
N.V. Kukhtarev, V.B. Markov, S.G. Odulov, M.S. Soskin, and V.L. Vinetskii, Ferroelectrics <u>22</u> , 949 (1979).	Analysis, LiNbO ₃
N.V. Kukhtarev, V.B. Markov, S.G. Odulov, M.S. Soskin, and V.L. Vinetskii, Ferroelectrics <u>22</u> , 961 (1979).	Analysis, LiNbO ₃
N. Kukhtarev and S. Odulov, Opt. Comm. <u>32</u> , 183 (1980).	LiNbO ₃ , LiTaO ₃
L.K. Lam, T.Y. Chang, J. Feinbert, and R.W. Hellwarth, to be published (1981).	BaTiO ₃
A.P. Levanyuk, E.M. Uyukin, V.A. Pashkov, and N.M. Soloveva, Sov. Phys. Sol. St. <u>22</u> , 675 1980).	LiNbO ₃
A.P. Levanyuk, A.R. Pogosyan, and E.M. Uyukin, to be published (1981).	LiNbO ₃
A. Marrakchi and J.P. Huignard, Appl. Phys. <u>24</u> , 131 (1981).	BSO

K. Megumi, H. Kozuka, M. Kubayashi, and Y. Furuhashi, Appl. Phys. Lett. 30, 631 (1977). SBN

F. Micheron, C. Mayeux, and J.C. Trotier, Appl. Opt. 13, 784 (1974). PLZT, SBN

M.G. Moharam and L. Young, J. Appl. Phys. 48, 3280 (1977). Analysis

S. Odulov, M. Soskin, and M. Vasnetsov, Opt. Comm. 32, 355 (1980) LiTaO₃

R. Orlowski and E. Kratzig, Solid State Comm. 27, 135X (1978). LiNbO₃, LiTaO₃

J.M. Spinhirne, D. Ang, C.S. Joiner, and T.L. Estle, Appl. Phys. Lett. 30, 90 (1977). LiTaO₃

D.L. Staebler and J.J. Amodei, J. Appl. Phys. 43, 104 (1972). LiNbO₃

D.L. Staebler and W. Phillips, Appl. Opt. 13, 788 (1974). LiNbO₃

J.B. Thaxter, Appl. Phys. Lett. 15, 210 (1969). SBN

J.B. Thaxter and M. Kestigian, Appl. Opt. 13, 913 (1974). SBN

R.L. Townsend and J.T. LaMacchia, J. Appl. Phys. 41, 5188 (1970). BaTiO₃

D. Von Der Linde, A.M. Glass, and K.F. Rodgers, Appl. Phys. Lett. 26, 22 (1975). KTN

J.O. White, Cronin-Golomb, B. Fischer, and A. Yariv, Appl. Phys. Lett., to be published (1981).

V.E. Wood, N.F. Hartman, and C.M. Verber, Ferroelectrics 27, 237 (1980). LiNbO₃

V.E. Wood, R.C. Sherman, N.F. Hartman, and C.M. Verber, Ferroelectrics 32, to be published (1981). LiNbO₃

L. Young, W.K. Y. Wong, M.L.W. Thewalt, and W.D. Cornish, Appl. Phys. Lett. 24, 264 (1974). LiNbO₃

END

FILMED

2-83

DTIC